# A new heuristic approach for contextuality degree estimates and its four- to six-qubit portrayals\*

Axel Muller\*, Metod Saniga\*, Alain Giorgetti\*, Frédéric Holweck<sup>†,‡,§</sup>, and Colm Kelleher<sup>†,‡</sup>

\*Université Marie et Louis Pasteur, CNRS, institut FEMTO-ST, F-25000 Besançon, France

\*Astronomical Institute of the Slovak Academy of Sciences, SK-05960 Tatranská Lomnica, Slovakia

<sup>†</sup>Université Marie et Louis Pasteur, UTBM, CNRS, Laboratoire Interdisciplinaire Carnot de Bourgogne ICB UMR 6303, 90010 Belfort, France

<sup>‡</sup>Université Bourgogne Europe, CNRS, Laboratoire Interdisciplinaire Carnot de Bourgogne ICB UMR 6303, 21000 Dijon, France §Department of Mathematics and Statistics, Auburn University, Auburn (AL), U.S.A.

#### Abstract

We introduce and describe a new heuristic method for finding an upper bound on the degree of contextuality and the corresponding unsatisfied (i. e., non-reproducible by any NCHV model) part of a quantum contextual configuration with three-element contexts (i. e., lines) located in a multi-qubit symplectic polar space of order two. While the previously used method based on a SAT solver was limited to three qubits, this new method is much faster and more versatile, enabling us to also handle four-to six-qubit cases. The method is illustrated by the structure of unsatisfied parts of the associated contextual configurations represented by quadrics and full spaces; these entail well-known finite geometries like the split Cayley hexagon of order two, the dual polar space of rank three and order two as well as certain incidence graphs of binary projective spaces of small dimensions.

<sup>\*</sup>Author version of [29], with a minor correction on Page 9, signaled in a footnote in red.

## 1 Introduction

A couple of years ago, de Boutray, Masson and three of the authors [5] introduced the notion of the degree of contextuality of a quantum configuration regarded as a particular sub-geometry of a multi-qubit symplectic polar space of order two and were already able to compute this degree for quadrics of the three-qubit space. In a later work [30], a more efficient SAT-based algorithm was proposed, together with an implementation in C language also able to partially handle the four-qubit case. Moreover, in selected three-qubit configurations, this new algorithm even allowed us to see *explicit* point-line geometries formed by the smallest number of unsatisfied contexts, these being – up to isomorphism – equal to (i) a set of nine mutually disjoint lines for an elliptic quadric, (ii) a set of 21 lines that can be identified with the edges of the Heawood graph for a hyperbolic quadric and, last but not least, (iii) a "classical" copy of the split Cayley hexagon of order two for the configuration comprising all the 315 contexts of the space.

In order to address in a similar vein quantum configurations with more than three qubits, we propose here a new heuristic approach. The approach is much faster and more versatile than the previous one, furnishing either new or considerably improved upper bounds on the degree of contextuality of configurations living in four- to seven-qubit spaces. In addition, in the four- to six-qubit spaces, it also provides a sufficiently detailed geometric understanding of the corresponding unsatisfied parts of contextual configurations under study.

The paper is organized as follows. We start with a brief inventory of the basic concepts and notations in Section 2, to be followed, in Section 3, by a detailed description of the new method and a brief tabular listing of the new results. Section 4 offers a chain of combinatorial geometric arguments to ascertain the lower bounds on the degree of contextuality for some specific generic cases. Section 5 deals with the geometrically-slanted description of the most important new results achieved and provides a fairy detailed illustration of those pertaining to the four-, five- and six- qubit spaces. Finally, in Section 6 one recollects the main achievements and outlines possible direction(s) of the future work, and in Section 7 we briefly address the significance of studying general N-qubit proofs of quantum contextuality and highlight other prospective applications of our heuristic method.

This heuristic method is implemented in the Qontextium software publicly available in a GitHub repository [27].

## 2 Background concepts and notations

This section revisits the connection between sets of mutually commuting N-qubit Pauli operators (N being a positive integer) and the totally isotropic subspaces in the symplectic polar space of rank N and order 2, W(2N-1,2), as referenced in [12,43,47]. The N-qubit Pauli group,  $\mathcal{P}_N$ , is the subset of  $GL_{2^N}(\mathbb{C})$  composed of the elements  $\mathcal{O}$  defined by

$$\mathcal{O} = sA_1 \otimes A_2 \cdots \otimes A_N, \text{ with } s \in \{\pm 1, \pm i\} \text{ and } A_k \in \{I, X, Y, Z\},$$
 (1)

where X, Y, Z are the standard Pauli matrices and I is the corresponding identity matrix. In the sequel, these elements will be shorthanded as  $\mathcal{O} = sA_1A_2\cdots A_N$ .

Given the fact that the Pauli matrices  $\{I, X, Y, Z\}$  are expressible through matrix multiplication of Z and X as

$$I = Z^{0}.X^{0} \leftrightarrow (0,0), \quad X = Z^{0}.X^{1} \leftrightarrow (0,1), Y = iZ^{1}.X^{1} \leftrightarrow (1,1), \quad Z = Z^{1}.X^{0} \leftrightarrow (1,0),$$
(2)

where the dot '.' stands for the ordinary matrix product, eq. (1) can be cast into the following form

$$\mathcal{O} = s(Z^{\mu_1}.X^{\nu_1})(Z^{\mu_2}.X^{\nu_2})\cdots(Z^{\mu_N}.X^{\nu_N}) \tag{3}$$

with  $s \in \{\pm 1, \pm i\}$  and  $\mu_i, \nu_j \in \{0, 1\}$ . The last expression leads to a surjective map between  $\mathcal{P}_N$  and  $\mathbb{F}_2^{2N}$  ( $\mathbb{F}_2$  being the smallest Galois field):

$$\pi : \begin{cases} \mathcal{P}_N \to \mathbb{F}_2^{2N} \\ \mathcal{O} = s(Z^{\mu_1}.X^{\nu_1})(Z^{\mu_2}.X^{\nu_2}) \cdots (Z^{\mu_N}.X^{\nu_N}) \\ \mapsto (\mu_1, \mu_2, \dots, \mu_N, \nu_1, \nu_2, \dots, \nu_N). \end{cases}$$
(4)

The center of  $\mathcal{P}_N$  is  $C(\mathcal{P}_N) = \{\pm I_N, \pm i I_N\}$ , where  $I_N$  is that particular element defined by eq. (1) for which  $A_1 = A_2 = \cdots = A_N = I$  and s = +1. Therefore,  $\mathcal{P}_N/C(\mathcal{P}_N)$  is isomorphic to the additive group  $\mathbb{F}_2^{2N}$ . Disregarding the neutral element, we then obtain a correspondence between equivalence classes of  $\mathcal{P}_N/C(\mathcal{P}_N)$  and points of PG(2N-1,2), the (2N-1)-dimensional projective space over the two-elements field

$$\underline{\pi}: \begin{cases} \mathcal{P}_N/C(\mathcal{P}_N) \setminus C(\mathcal{P}_N) \to \operatorname{PG}(2N-1,2) \\ \overline{\mathcal{O}} = \{s(Z^{\mu_1}.X^{\nu_1})(Z^{\mu_2}.X^{\nu_2}) \cdots (Z^{\mu_N}.X^{\nu_N})\} \\ \mapsto [\mu_1: \mu_2: \cdots: \mu_N: \nu_1: \nu_2: \cdots: \nu_N]. \end{cases}$$
(5)

Here, the projective space  $\operatorname{PG}(2N-1,2)$  is the geometry whose points can be represented by (2N)-tuples of the form  $(x_1,x_2,x_3,\ldots,x_{2N})$  where  $x_i\in\mathbb{F}_2$ , disregarding the trivial  $(0,0,0,\ldots,0)$ -tuple, and whose subspaces (i. e., lines, planes, etc.) represent sets of points whose coordinates  $x_i$ 's meet specific linear constraints. In  $\mathcal{P}_N/C(\mathcal{P}_N)$  two classes  $\overline{\mathcal{O}}$  and  $\overline{\mathcal{O}'}$  commute if and only if  $\sum_{i=1}^N \mu_i \nu_i' + \mu_i' \nu_i = 0$ , with  $\mathcal{O} = s(Z^{\mu_1}.X^{\nu_1})(Z^{\mu_2}.X^{\nu_2})\ldots(Z^{\mu_N}.X^{\nu_N})$  and  $\mathcal{O}' = s'(Z^{\mu_1'}.X^{\nu_1'})(Z^{\mu_2'}.X^{\nu_2'})\ldots(Z^{\mu_N}.X^{\nu_N'})$  being representatives of either class. To account for these commutation relations, we introduce on  $\operatorname{PG}(2N-1,2)$  a non-degenerate symplectic form:

$$\langle p, q \rangle = \sum_{i=1}^{N} p_i q_{N+i} + p_{N+i} q_i, \tag{6}$$

with  $p = [p_1 : p_2 : \cdots : p_{2N}]$  and  $q = [q_1 : q_2 : \cdots : q_{2N}]$ . The consequence is that two (classes of pairwise) commuting observables in  $\mathcal{P}_N/C(\mathcal{P}_N)$  define a totally isotropic line in  $\mathrm{PG}(2N-1,2)$  with respect to this symplectic form or, in other words, the commutation relations are now encoded into specific collinearity relations on such a  $\mathrm{PG}(2N-1,2)$ , which also has the proper name:

**Definition 1.** The space of totally isotropic subspaces of PG(2N-1,2) equipped with a non-degenerate symplectic form  $\langle , \rangle$  is called the symplectic polar space of rank N and order two, usually denoted as W(2N-1,2).

<sup>&</sup>lt;sup>1</sup>A totally isotropic subspace of PG(2N-1,2) equipped with a non-degenerate symplectic form is any subspace on which the symplectic form vanishes identically; a totally isotropic subspace of maximal (projective) dimension N-1 is called a generator of W(2N-1,2).

The smallest non-trivial space, N=2, often called the *doily*, is notable in the sense that it is also the smallest thick generalized quadrangle [31] and the sole out of 245 342 15<sub>3</sub>-configurations that is triangle-free [38].

Viewed as a point-line incidence structure, W(2N-1,2) contains

$$|\mathcal{W}|_{p} = 4^{N} - 1 \tag{7}$$

points and

$$|\mathcal{W}|_l = (4^N - 1)(4^{N-1} - 1)/3 \tag{8}$$

lines, with three points per line and  $4^{N-1} - 1$  lines through a point. Given a point of W(2N-1,2), then the lines, planes, ..., and generators passing through this point form a geometry isomorphic to W(2N-3,2). Moreover, W(2N-1,2) contains two specific types of subgeometries, hyperbolic and elliptic quadrics, that are of particular importance regarding the study of contextual configurations [5]:

1. **Hyperbolic Quadric**  $Q^+(2N-1,2)$ : For  $N \ge 1$ , it is defined by the standard canonical equation:

$$x_1x_{N+1} + x_2x_{N+2} + \dots + x_Nx_{2N} = 0.$$

Each  $Q^+(2N-1,2)$  is endowed with  $(2^{N-1}+1)(2^N-1)$  points and there are  $(2^{N-1}+1)(2^N-1)+1$  copies of them in  $\mathcal{W}(2N-1,2)$ .

2. Elliptic Quadric  $Q^-(2N-1,2)$ : For  $N \geq 2$ , it consists of all points and subspaces in W(2N-1,2) that satisfy the standard equation:

$$f(x_1, x_{N+1}) + x_2 x_{N+2} + \dots + x_N x_{2N} = 0,$$

where f is an irreducible polynomial over  $\mathbb{F}_2$ . Each  $Q^-(2N-1,2)$  contains  $(2^{N-1}-1)(2^N+1)$  points and in  $\mathcal{W}(2N-1,2)$  there are  $(2^{N-1}-1)(2^N+1)+1$  copies of these configurations.

In what follows, we will select from each equivalence class of  $\mathcal{P}_N/C(\mathcal{P}_N)$  a single representative, namely the canonical one (s=1), to label a particular point of  $\mathcal{W}(2N-1,2)$ . A canonical observable  $\mathcal{O}$  is either symmetric ( $\mathcal{O}^{T} = \mathcal{O}$ ), or skew-symmetric ( $\mathcal{O}^{T} = \mathcal{O}$ )  $-\mathcal{O}$ ; an observable is symmetric if the corresponding tensor product (see eq. (1)) features an even (including zero) number of Y's; otherwise it is skew-symmetric. Also, in order to check whether two different N-qubit observables commute it is not necessary to check the (two-way) product of the corresponding  $2^N \times 2^N$  matrices. It suffices to simply count the number of places in which they feature different Pauli matrices; if this number is even the observables commute, if it is odd they do not. It then can be shown that given a canonical observable  $\mathcal{O}$ , the set of symmetric canonical observables commuting with  $\mathcal{O}$  together with the set of skew-symmetric observables not commuting with  $\mathcal{O}$  lie on a quadric of  $\mathcal{W}(2N-1,2)$ , this quadric being hyperbolic (resp. elliptic) if O is symmetric (resp. skew-symmetric). We call this associated observable the *index* of a quadric and can express it, if appropriate, in a subscript,  $\mathcal{Q}_{\mathcal{O}}^{\pm}(2N-1,2)$ , noting that there exists a particular hyperbolic quadric associated with  $I_N$ ,  $\mathcal{Q}_{I_N}^+(2N-1,2)$ . It is worth stressing here that this property enables us to find all the observables belonging to a particular quadric without even making use of its abstract algebraic equation and

projective coordinates. Thus, for example, a four-qubit hyperbolic quadric  $Q^+(7,2)$  (respectively a four-qubit elliptic quadric  $Q^-(7,2)$ ) comprises 135 (respectively 119) four-qubit observables subject to the above-introduced commutation relations with a given symmetric (respectively skew-symmetric) four-qubit observable; moreover, through any observable of  $Q^+(7,2)$  (resp.  $Q^-(7,2)$ ) there pass 35 (resp. 27) lines lying fully on the quadric and touching a certain  $Q^+(5,2)$  (resp.  $Q^-(5,2)$ ) belonging to the quadric. Also, when referring in the sequel to W(2N-1,2) we will always have in mind the W(2N-1,2) with its points being labelled by canonical N-qubit observables as dictated by eqs. (4) and (5). Moreover, a line (or any other linear subspace) of such a multi-qubit W(2N-1,2) will be called positive or negative according as the (ordinary) product of the observables located in it is  $+I_N$  or  $-I_N$ , respectively. In order to quickly find the sign of a context one simply takes the bit-wise products of the corresponding Pauli matrices and the identity matrix and then multiplies the phases obtained; for example, the three-qubit line consisting of the observables XYZ, ZIX and YYY is positive as XYZ. ZIX.  $YYY = (X.Z.Y)(Y.I.Y)(Z.X.Y) = (-iI)(+I)(+iI) = +I^{\otimes 3}$ .

Next, given an even-dimensional projective space over  $\mathbb{F}_2$ , PG(2N,2), N > 1, a parabolic quadric in this space, Q(2N,2), is defined by the following canonical equation

$$x_1x_{N+1} + x_2x_{N+2} + \dots + x_Nx_{2N} + x_{2N+1}^2 = 0.$$

Any such quadric has a notable property that all its tangent hyperplanes pass through the same point (see, e.g., [7,16,20]), which is usually referred to as the *nucleus* of the quadric. Another well-known fact is (see, e.g., [15,16]) that

$$\mathcal{W}(2N-1,2) \cong \mathcal{Q}(2N,2).$$

In order to distinguish between these two cases, we shall call – following the notation of [41] – the  $\mathcal{W}(2N-1,2)$  embedded into  $\mathrm{PG}(2N-1,2)$  a linear  $\mathcal{W}(2N-1,2)$ , whereas the space represented by  $\mathcal{Q}(2N,2)$  in  $\mathrm{PG}(2N,2)$  will be referred to as a quadratic  $\mathcal{W}(2N-1,2)$ . It is worth mentioning that the intersection of a  $\mathcal{Q}^+(2N-1,2)$  and a  $\mathcal{Q}^-(2N-1,2)$  is isomorphic to a quadratic  $\mathcal{W}(2N-3,2)$  (see, e.g., [50]). By way of example, there are 120 (resp. 136) quadratic  $\mathcal{W}(5,2)$ 's located in any  $\mathcal{Q}^+(7,2)$  (resp.  $\mathcal{Q}^-(7,2)$ ) of  $\mathcal{W}(7,2)$ , these being in a bijection with the set of off-quadric observables; in particular, given an off-quadric observable, there exists a unique  $\mathcal{W}(5,2)$  in  $\mathcal{Q}^+(7,2)$  (resp.  $\mathcal{Q}^-(7,2)$ ) such that each of its 63 observables commutes with this particular off-quadric observable, which is, in fact, nothing but the nucleus of this  $\mathcal{W}(5,2)$ .

We shall also employ the notion of a finite point-line incidence structure  $C = (P, L, \in)$ , where P and L are, respectively, finite sets of points and lines and where  $\in$  is a binary relation between P and L, indicating which point-line pairs are incident; the number of lines of C incident with a point of C will be called the *degree* of the point. Any distinguished subset of P such that a line of L is either fully contained in it or shares with it just a single point is called a *geometric hyperplane* of C [39].

Given W(5,2), its dual space,  $\mathcal{D}W(5,2)$ , as a point-line incidence structure, has for its points the 135 planes of W(5,2) and for its lines the 315 lines of W(5,2), the incidence being containment (see, e.g., [37]). As a plane of W(5,2) has seven lines, there are seven lines passing through a point of  $\mathcal{D}W(5,2)$ ; and as there are three planes sharing a line in W(5,2), each line of  $\mathcal{D}W(5,2)$  features three points. Hence,  $\mathcal{D}W(5,2)$  is a specific  $(135_7,315_3)$ -configuration. We also mention that  $\mathcal{D}W(5,2)$  contains 63 W(3,2)'s, three sharing a line and seven through a point; each such doily is, as a

point-line incidence structure, represented by 15 planes and 15 lines passing via the same point of W(5,2), the incidence being containment.

Another relevant geometry associated with W(5,2) is the split Cayley hexagon of order two,  $\mathcal{H}$ , which is a  $(63_3)$ -configuration whose smallest polygons are hexagons (see, e.g., [36]). It is embeddable into W(5,2) in two different ways, called classical and skew [3]. A classically-embedded hexagon,  $\mathcal{H}_{\mathcal{C}}$ , possesses in W(5,2) a much greater symmetry than its skew-embedded cousin,  $\mathcal{H}_{\mathcal{S}}$ . To see this, let us call a point of  $\mathcal{H}$  embedded in W(5,2) planar if all the three lines passing through it lie in the same plane of W(5,2). An  $\mathcal{H}_{\mathcal{C}}$  is characterized by the fact that each of its points is planar. In an  $\mathcal{H}_{\mathcal{S}}$ , only 15 points have this property; they are situated on three pairs of concurrent lines, the three points of concurrence lying themselves on a line – the latter called the axis of  $\mathcal{H}_{\mathcal{S}}$ . There are altogether 120  $\mathcal{H}_{\mathcal{C}}$ 's and 7560  $\mathcal{H}_{\mathcal{S}}$ 's in a W(5,2), as first ascertained by a computer-aided search in [17] and later given a computer-free, geometric-combinatorial substantiation in [42].

We will also encounter several distinguished graphs. Here we define two (families) of them, which are both bipartite and closely related to each other. The first is a point-hyperplane incidence graph of PG(d,2),  $d \ge 1$ . The vertices of this graph are both points and hyperplanes (i. e., subspaces of maximal dimension) of PG(d,2), where a vertex represented by a point is connected to a vertex represented by a hyperplane iff the point belongs to the hyperplane. The other is the Haar graph of a positive integer n, H(n) (see, e. g, [51]), defined as follows. Let us consider a binary representation of n,

$$n = b_{k-1}2^{k-1} + b_{k-2}2^{k-2} + \dots + b_12^1 + b_0$$

where  $(b_{k-1}, b_{k-2}, \ldots, b_1, b_0)$ , with  $b_{k-1} = 1$ , is the binary vector of n. A graph H(n) has two disjoint vertex sets  $u_i$  and  $v_i$ ,  $i = 0, 1, 2, \ldots, k-1$ , with  $u_i$  being adjacent to  $v_{i+j}$  if and only if  $b_j = 1 \pmod{k}$ . Interestingly, each point-hyperplane incidence graph of PG(d, 2) is also a Haar graph; for example, the famous Heawood graph, aka the point-line incidence graph of PG(2, 2), is isomorphic to H(69).

Finally, in the context of this paper, a quantum configuration is a pair (O, C) where  $O = \{M_1, \ldots, M_p\}$  is a set of p = |O| canonical Pauli observables, here identified with points of a multi-qubit  $\mathcal{W}(2N-1,2)$ , and  $C = \{c_1, \ldots, c_l\}$  is a set of l = |C| contexts, here limited to lines of  $\mathcal{W}(2N-1,2)$ . Its incidence matrix  $A \in \mathbb{F}_2^{l \times p}$  is defined by  $A_{i,j} = 1$  if the *i*-th context  $c_i$  contains the *j*-th observable  $M_j$ . Otherwise,  $A_{i,j} = 0$ . Its valuation vector  $E \in \mathbb{F}_2^l$  is defined by  $E_i = 0$  if the line  $c_i$  is positive and  $E_i = 1$  if it is negative. Then the degree of contextuality of (O, C) is d defined [5] by

$$d = d_H(E, \operatorname{Im}(A)), \tag{9}$$

where  $d_H$  is the Hamming distance on the vector space  $\mathbb{F}_2^l$ .

Given a quantum configuration K = (O, C), one can associate with it a configuration  $\widetilde{K}$  that is geometrically identical with K, but has its observables replaced by +1's and -1's by an assignment function  $a: O \to \{-1, +1\}$  and the sign of each context  $c \in C$  replaced by the product  $\Pi_{M \in c}$  a(M) of these +1's and -1 over its members. Given the K and a  $\widetilde{K}$ , the configuration with the same points/observables and consisting of those contexts of K that have different signs than the corresponding lines in  $\widetilde{K}$  is called an unsatisfied configuration of K and is denoted as  $\widetilde{K}^{\text{uns}}$ ; in other words,  $\widetilde{K}^{\text{uns}}$  is that part of K that cannot be reproduced by non-contextual hidden-variable (NCHV) theories (i. e., those theories in which the values of the physical observables are the same irrespectively of the experimental context which they belong to).

In what follows, we will use special symbols  $E_N^{\rm uns}$ ,  $H_N^{\rm uns}$  and  $F_N^{\rm uns}$ , with N>1, for an unsatisfied configuration of  $\mathcal{Q}^-(2N-1,2)$ ,  $\mathcal{Q}^+(2N-1,2)$  and of the configuration consisting of all lines of  $\mathcal{W}(2N-1,2)$ , respectively. For a given K there are, of course, a (large) number of  $\widetilde{K}$ 's differing from each other in the distribution of +1's and -1's across their points and so, in general, several associated (mutually non-isomorphic)  $\widetilde{K}^{\rm uns}$ 's.

From Formula (9) it follows that the degree of contextuality  $d_K$  of the quantum configuration K is also the minimal number of unsatisfiable contexts in it, in other words the number of contexts in any unsatisfied configuration  $\widetilde{K}^{\text{uns}}$  of K of minimal size. So, to determine the contextuality degree  $d_K$  of K, it is sufficient to find out such an unsatisfied configuration  $\widetilde{K}^{\text{uns}}$  that has the *smallest* possible number of contexts, with  $d_K$  then being this number of contexts. Obviously, the particular  $\widetilde{K}$  all of whose points are labelled by +1's gives  $\widetilde{K}^{\text{uns}}$  whose contexts correspond solely to the negative contexts of K, thus providing the number of negative contexts of K as a natural *upper* bound for  $d_K$ . Hence, our primary, and almost exclusively computer-aided, effort will be focused on discerning those  $\widetilde{K}^{\text{uns}}$ 's that have a (possibly much) smaller number of contexts than the number of negative contexts in K and which thus furnish (considerably) reduced upper bounds on the value of  $d_K$ .

# 3 Novel computer-aided heuristics for ascertaining an upper bound on the contextuality degree

### 3.1 Contextuality of quantum configurations

A quantum configuration K is contextual if its degree of contextuality d, as defined by formula (9), is different from zero. The problem of finding d can be formulated as an optimization problem, namely the maximization of satisfied contexts in K. As already described in Section 2, it can be addressed by looking for an associated unsatisfied configuration  $\widetilde{K}^{\text{uns}}$  that has the maximal possible number of contexts with the same sign as in K. The conjunction of these sign constraints can be expressed as a system of linear equations over  $\mathbb{F}_2$  [30]. The problem of maximizing the number of valid equations of this kind is known as Max-E3-Lin-2 [19], when each equation contains exactly three variables. When the sign constraints are encoded as XOR clauses, the optimization problem is the MAX-XOR-SAT problem [25]. Either way, in the general case, solving these problems is known to be in the class APX of problems for which there is a polynomial-time algorithm able to find an approximation of the solution (within a given performance ratio) [25].

A first method by Trandafir et. al. [48], which approached this problem in a linear code perspective, managed to compute this bound for quantum configurations up to three qubits. In this approach a function of the language Magma is used, that computes a weight distribution of a linear code, and which has an exponential complexity in the dimension of the row space of the incidence matrix of the configuration. However, thanks to the MacWilliams identity, this complexity becomes the lowest value c between the dimensions and codimensions of that row space. As expected, we can see in Figure 2

that incrementing c doubles the computing time, making the computation for matrices whose minimum is 42 or higher longer than one hour.

To move further, we, therefore, give up accuracy and experiment with approximation methods. Our first approximate method is the already-mentioned SAT-based approach interrupted before checking minimality, hereafter denoted as SAT(a). Then we consider a large collection of off-the-shelf heuristic-based methods implemented in the Google OR-Tools [32]. These tools find optimal solutions for up to three qubits, by using local and core-based (which focus on solving a critical subset of the problem to enhance computational efficiency) approaches, and provide some better bounds for four qubits than a SAT solver alone within a reasonable time frame. However, they fail to provide any useful results for five qubits and more. Therefore, we have designed and implemented a new approximation algorithm presented and evaluated in the rest of this section.

### 3.2 Optimization algorithm

For geometries with more qubits, we suspected that specific heuristics based on some particular properties of the geometry could yield improved bounds. Since these geometries often exhibit symmetries, we designed and present in this section a heuristic grouping variables by the number of unsatisfied constraints they are part of.

Given a quantum configuration K = (O, C) and its valuation vector E, Algorithm 1

#### **Algorithm 1** Optimize Hamming Distance

```
1: function OPTIMIZE_HAMMING_DISTANCE(O, C, E)
        for o \in O do
 2:
            a[o] \leftarrow 1
 3:
            uns[o] \leftarrow number of contexts containing o unsatisfied by a
 4:
        end for
 5:
        min_a \leftarrow a
 6:
        for i \leftarrow 1 to MAX\_ITERATIONS do
 7:
            for o \in O do
 8:
                if uns[o] > \theta \times max(uns) and random() < \gamma then
 9:
                    a[o] \leftarrow -a[o]
10:
                    for each context c such that o \in c do
11:
                        sign \leftarrow \Pi_{m \in c} \ a[m]
12:
                        for each m \in c do
13:
                             uns[m] \leftarrow uns[m] - E_c \times sign
14:
                        end for
15:
                    end for
16:
                end if
17:
            end for
18:
            if d_H(a, E) < d_H(min_a, E) then min_a \leftarrow a
19:
        end for
20:
        return min_a
21:
22: end function
```

performs a stochastic local search for its optimum Hamming distance, as expressed by Formula (9). Its local variables a and  $min_{-}a$  of type  $O \to \{-1, +1\}$  are two assignment functions. The second array  $min_{-}a$  stores the best assignment currently found by the algorithm. The first array a stores a candidate for a better solution. It is initialized to 1 for each  $o \in O$ , on Line 3. For each  $o \in O$  the local variable  $uns: O \to \mathbb{N}$  stores the number uns[o] of contexts containing o that are left unsatisfied by a. Therefore, it is initialized by the number of negative contexts through o, on Line 4.

To illustrate the algorithm in a graphical way, let us consider – as a particularly apt example – a two-spread of a quadratic four-qubit doily, as depicted in Figure 1. Let us recall (see, for example, [35]) that a two-spread of a doily is a  $(15_2, 10_3)$ -configuration that we get if we remove from the doily any set of five pairwise disjoint lines. It was already proved [30] that a multi-qubit two-spread is a contextual quantum configuration whose degree of contextuality is one. Our selected four-qubit two-spread features five negative lines, namely those highlighted by double red lines. The three two-spread assignments (a), (b) and (c) and the corresponding rows in the table incorporated in Figure 1 show the three steps of an execution of the algorithm.

The algorithm is parameterized by the threshold  $\theta$  on the number of unsatisfied contexts an observable is in for it to have its value possibly changed, relatively to the maximal number  $\max(uns)$  of unsatisfied contexts in the current assignment. By swapping the sign (Line 10) of most of the observables which satisfy this criterion (Line 9), the algorithm can significantly reduce the Hamming distance of the whole configuration. For instance, in the example of execution depicted in Figure 1, the value 0.8 has been chosen for  $\theta$ . In the initial state (a), it is visible in the first row of the table and in the first subfigure that the maximal number of unsatisfied contexts per observable is two, which means that only observables pertaining to two unsatisfied contexts will be considered since  $2 \ge 0.8 \times 2$ , but  $1 < 0.8 \times 2$  and  $0 < 0.8 \times 2$ .

The second parameter of the algorithm is a sign flip probability  $\gamma$  for selected observables to have their signs flipped. On Line 9 this value is compared 2 to the result of the random() function that uniformly returns a random real number between 0 and 1. This addition of randomness significantly reduces the observed issue of cycling over a too small subset of visited assignments. In the example in Figure 1 the chosen value for  $\gamma$  is 0.7.

Every time the sign a[o] of an observable o is flipped (Line 10), the number uns[m] of unsatisfied contexts of each observable m sharing a context c with o is updated (Lines 11-16). First, the new sign of the context c is computed on Line 12. Then, the number of unsatisfied contexts uns[m] is decremented if this sign is the expected one  $E_c$ , meaning that the context is now satisfied, and incremented otherwise (Line 14).

Once the whole assignment has been changed, the Hamming distance between it and the valuation vector is computed. If this distance is the smallest found thus far, the assignment is stored. This process continues until the number of iterations exceeds  $MAX\_ITERATIONS$ . The purpose of this limit is to prevent an infinite loop. Finally, this algorithm returns the best assignment  $min\_a$  that was found, from which the corresponding unsatisfied configuration  $\widetilde{K}^{uns}$  can easily be computed. In the example in Figure 1, since the algorithm starts by assigning to each observable the value +1, the only initially unsatisfied contexts are the five negative lines (dashed in Figure 1(a)). There are four observables featuring two, i. e., the maximal number of unsatisfied con-

<sup>&</sup>lt;sup>2</sup>The right comparison random()  $< \gamma$  here fixes the wrong one (random()  $> \gamma$ ) published in [29].

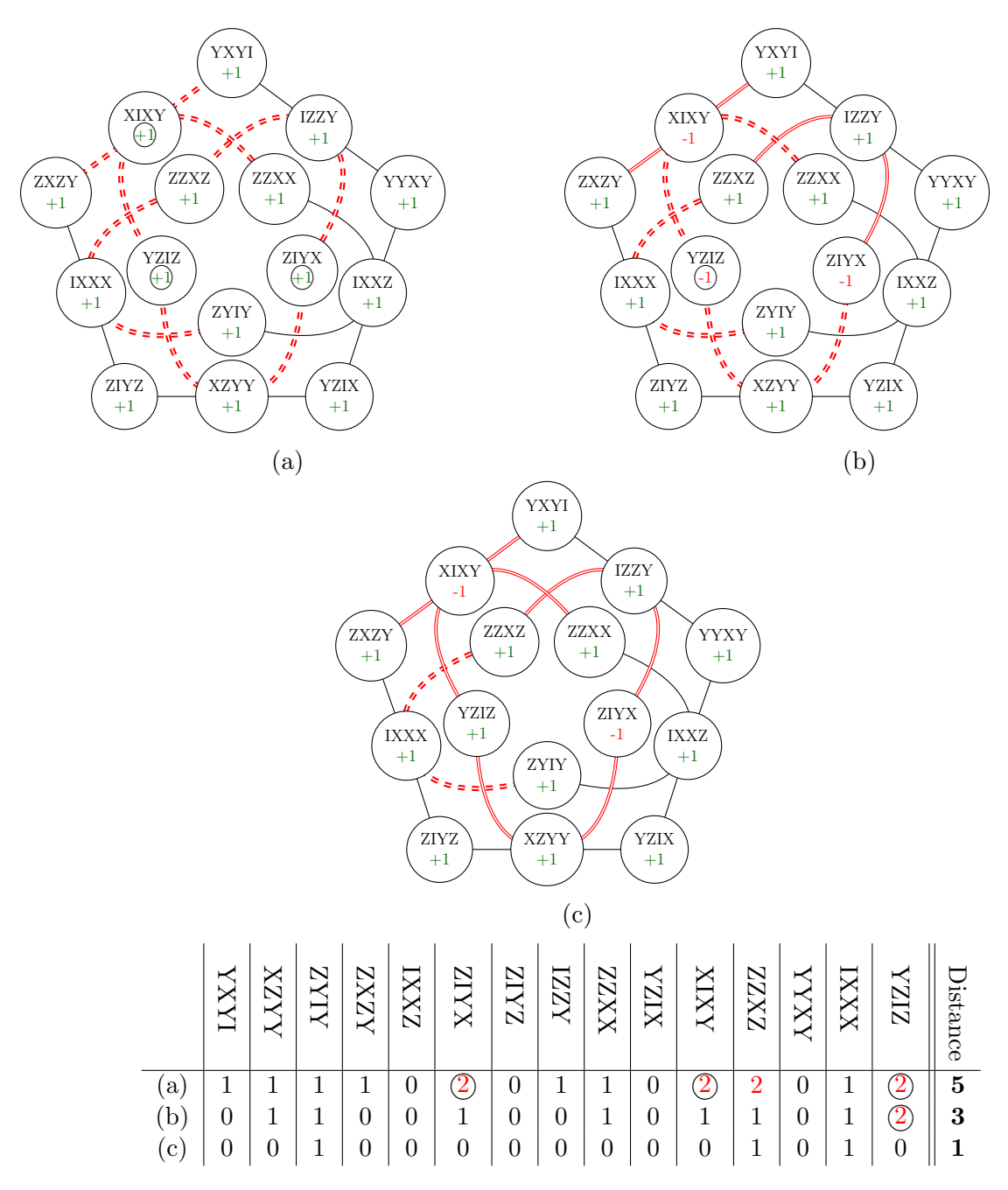


Figure 1: Graphical illustration of the successive steps of the algorithm on a two-spread, showing the sign assigned to each observable and in the associated table the number of unsatisfied contexts (dashed lines) containing it. The negative contexts are represented by the double lines colored in red. The value +1 is first assigned to all 15 observables (a). The last step (c) reaches the minimal possible distance for this geometry. In this example, the threshold  $\theta$  is 0.8 and the sign flip probability  $\gamma$  is 0.7.

texts passing through each of them, as also listed for the reader's convenience in the table at the bottom of the figure. In the next step, we flip the value from +1 to -1 at three of them, as indicated by circles in Figure 1(a) and the associated table as well.

With this changed labeling we find that at this step only three contexts are unsatisfied, as shown in Figure  $\mathbf{1}(b)$ . As now there is only one observable, namely YZIZ, that is on two unsatisfied contexts, we just need one more step to get the final result, Figure  $\mathbf{1}(c)$ , where only one context remains unsatisfied. It is worth noting that while every assignment given of a given loop iteration in this example has a lower Hamming distance than the preceding one, this is not always the case generally.

#### 3.3 Parameter optimization

Benchmarks were conducted on a variety of configurations in order to determine the most appropriate ways to adjust the values of the two parameters of Algorithm 1, namely the threshold  $\theta$  and the sign flip probability  $\gamma$ . This experimental study and its conclusions are summarized in B. Based on these conclusions, we chose to fix the value of  $\gamma$  at 0.97 and to adjust dynamically the value of  $\theta$  as detailed in the next paragraph.

The experimental study suggests that the best values of  $\theta$  lie in a subinterval of [0...1] whose boundaries differ significantly according to the input configuration. This led us to develop the following principles for the dynamic adjustment of this parameter  $\theta$ . Algorithm 1 is executed in parallel on several threads, with different values of  $\theta$  uniformly distributed between 0 and 1. At the end of each of its iterations, each thread displays the best Hamming distance value it found in a shared variable, if this value improves the best global value already found and stored in this variable. Every five iterations, a dedicated thread revises the interval of values for  $\theta$  as follows: its center becomes the value of  $\theta$  which has given the best distance until then and its width becomes half of that of the preceding interval. When the width of this interval reduces to 0.01 or less, i.e., after  $8 \times 5 = 40$  iterations, this interval is restored to [0...1], this is done in case the algorithm gets stuck with a sub-optimal value of  $\theta$ .

#### 3.4 New results

Our algorithm was run on the set of all lines of W(2N-1,2),  $3 \leq N \leq 7$ , on a number of specific subsets of lines of W(5,2) as well as on one of its elliptic and hyperbolic quadrics, since all the other ones have the same degree of contextuality. It has indeed recently been shown [26,48] that given an abstract configuration endowed with specific observables and contexts (for example, the doily endowed with two-qubit observables), any other admissible quantum assignment of this configuration (e.g., any doily located in the multi-qubit W(2N-1,2), for any N>2) will yield the same degree of contextuality. Hence, when checking for contextuality of a particular geometry it suffices to consider its simplest (i.e., with lowest number of qubits) quantum assignment.

The main new results are collected in Table 1 for configurations comprising all the lines of the corresponding space and in Table 2 for quadrics; in these tables, p is the number of observables, l is the total number of contexts and  $l^-$  is the number of negative contexts in a given configuration. For each quantum configuration, the same algorithm was run on 200 threads, from which the best assignment was then selected. The parameters  $\theta$  and  $\gamma$  were adjusted as described in Section 3.3. The duration is the time taken by the algorithm to find the displayed value or bound for the contextuality

degree of d, after running the algorithm for ten minutes up to six qubits, and for two hours for seven qubits. The improved upper bounds are highlighted in **bold font**.

N	p	l	$l^-$	d	Duration
2	15	15	3	3	$0.01 \; { m s}$
3	63	315	90	63	0.1 s
4	255	5 355	1908	$\leq 1575$	0.1 s
5	1023	86 955	35 400	$\leq 31479$	1 s
6	4095	1396395	615 888	$\leq \mathbf{553140}$	2 mn
7	16383	22362795	10352160	$\leq 9405663$	1 h 34 mn

Table 1: Exact values or specific upper bounds for the contextuality degree d of quantum configurations isomorphic to the configuration whose contexts are all the lines of W(2N-1,2), for  $3 \le N \le 7$ .

Quadric	N	p	l	l-	$ K^- $	d	Duration
Hyperbolic	2	9	6	1 or 3	9 or 1	1	0
Hyperbolic	3	35	105	27 or 39	27 or 9	21	0
Hyperbolic	4	135	1 575	532 or 604 or 612	81 or 54 or 1	$\leq 315$	0.01 s
Hyperbolic	5	527	23715	9 420 or 9 852 or 9 900	243 or 270 or 15	$\leq 6975$	0.2 s
Hyperbolic	6	2 0 7 9	365211	159 376 or 161 968 or 162 256 or 162 288	729 or 1 215 or 135 or 1	$\leq 132391$	2 s
Hyperbolic	7	8 255	5 720 715	2 636 592 or 2 652 144 or 2 653 872 or 2 654 064	2 187 or 5 103 or 945 or 21	$\leq 2331191$	3  mn  20  s
Elliptic	2	5	0	0	6	N/A	0
Elliptic	3	27	45	9 or 13	1 or 27	9	0
Elliptic	4	119	1071	360 or 384	12 or 108	$\leq$ 315	0.01 s
Elliptic	5	495	19635	7860 or 7876 or 8020	1 or 90 or 405	$\leq 7087$	$0.2 \mathrm{\ s}$
Elliptic	6	2 015	332475	145 920 or 146 016 or 146 880	18 or 540 or 1 458	$\leq 131700$	20 s
Elliptic	7	8 127	5458635	2 523 024 or 2 523 088 or 2 523 664 or 2 528 848	1 or 189 or 2835 or 5103	$\leq 2294580$	16 mn

Table 2: Known results for the exact values and **new** results for upper bounds of the contextuality degree d of quadrics. The notations are the same as in Table 1 apart from the new symbol  $|K^-|$  that stands for the number of quadrics having, respectively, a particular number of negative contexts listed in column  $l^-$ .

Other new values for the contextuality degree can be found in Table 4 in C, for the other subsets of three-qubit lines considered in the following performance study.

## 3.5 Performance analysis

This section presents a comparison of the computation time of our algorithm with the other approaches presented in Section 3.1 to approximate or exactly compute the contextuality degree of various quantum configurations. It is based on the experimental data presented in C.

Figure 2 shows a graph of the computation time of the exact methods for configurations of three-qubit lines given in the first and third blocks of Table 4. The x-axis represents the number of contexts/lines of the configuration and the y-axis displays the computation time in seconds on an exponential scale. This graph allows us to see the performance limit of each approach, clearly implying the necessity of using heuristics

for larger configurations. The Magma approach hits its limit first, followed by the SAT-based approach and then by the OR-Tools-based approach.

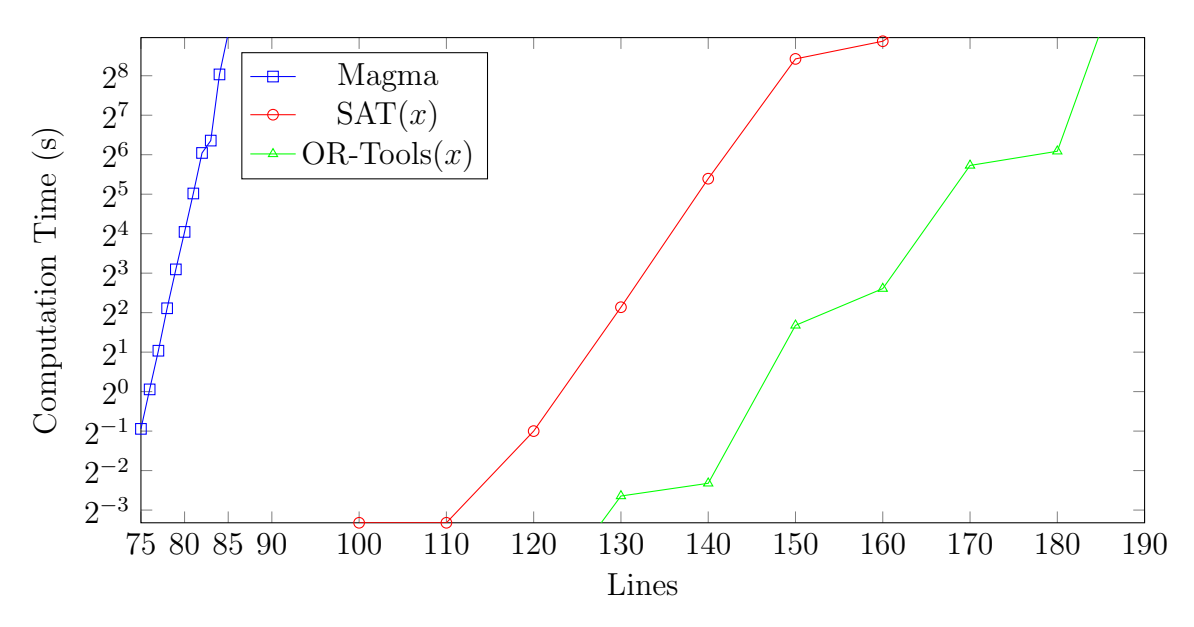


Figure 2: Computation time of different exact methods as a function of the number l of first lines of W(5,2) in lexicographic order.

The Magma approach computes a weight distribution, which has an exponential complexity in the dimension of the incidence matrix of the configuration. Thanks to the MacWilliams identity, this complexity becomes  $2^{min(dim,codim)}$ , related to the lowest value min(dim,codim) between the dimension and the codimension of this matrix [49]. As expected, we can see in the seventh column of Table 4 that incrementing min(dim,codim) doubles the computation time. The computation with matrices whose minimum is 42 or higher is longer than one hour.

SAT solving is theoretically NP-complete and can have exponential execution time in the worst case. However, implementing heuristics, conflict-driven clause learning and pruning techniques into modern SAT solvers often enable them to find solutions quickly for large, real-world problems. As shown in the columns Magma and SAT(x) for the first block of rows in Table 4 in C, the SAT-based approach is capable of solving the contextuality degree problem even for larger quantum configurations where the Magma-based approach already fails. The exponential complexity of the Magma-and SAT-based approaches is clearly discernible from Figure 2.

The column OR-Tools(x) of Table 4 shows that the OR-Tools find the minimal Hamming distances for all the considered three-qubit configurations, but not for the full set of lines, and find them faster than the SAT-based approach for three qubits, as shown more clearly in Figure 2. The OR-Tools approach indeed combines multiple algorithms to solve combinatorial optimization problems, including SAT solvers, making its performance comparable to that of the SAT-based approach, and sometimes significantly better. One notable exception is the whole set of three-qubit lines where the SAT-based approach takes, quite surprisingly, a very short time to compute the contextuality degree, in particular shorter than with the OR-Tools. We suspect that this has something to do with some extra symmetries characterizing this space.  $\mathcal{W}(5,2)$ 

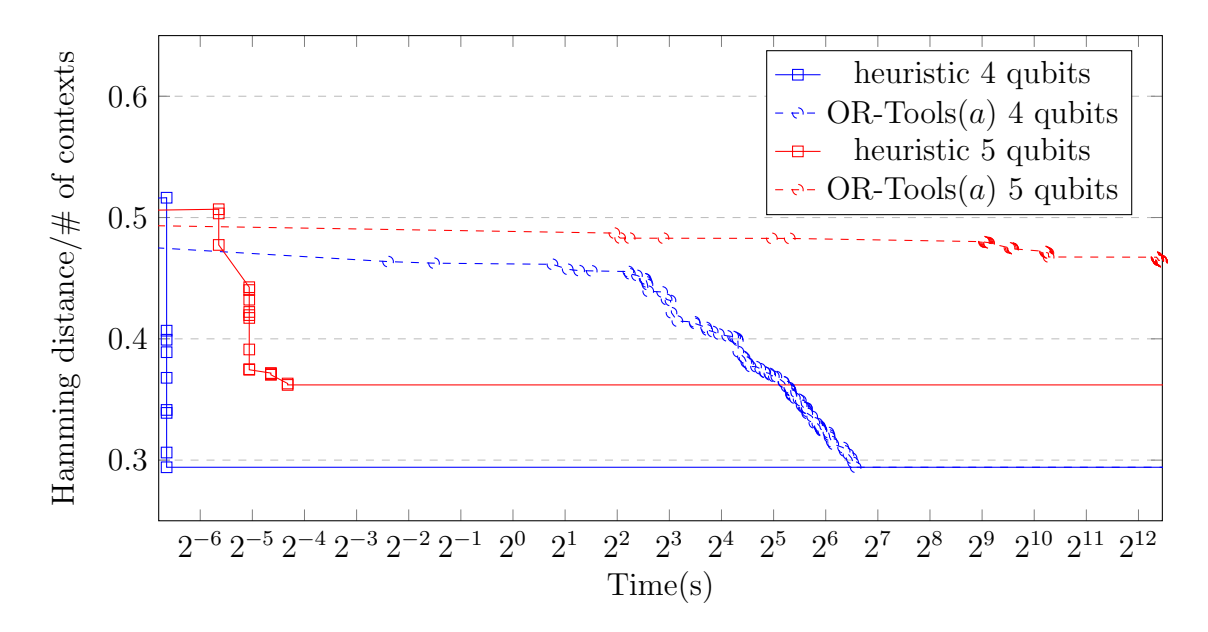


Figure 3: Minimal computed Hamming distance per context as a function of the computation time in seconds (shown in an exponential scale), for the full set of lines of W(7,2) (blue) and W(9,2) (red), using the heuristic (solid) and the OR-Tools (dashed) solver.

is, for example, the *only* space where the maximum number of mutually commuting observables (forming a Fano plane) is the same as that of pairwise anti-commuting ones (forming a Conwell heptad).

However, the SAT- and OR-Tools-based approaches fail to provide any exact result for four qubits and more (see the last six rows of Table 4 in  $\mathbb{C}$ ). As shown in the last two blocks of rows, for larger configurations, typically those with more than three qubits, the heuristic approach can provide a solution in a reasonable time, and although the OR-Tools(a) approach can also provide a solution, it is much slower and becomes unable to provide better results than the heuristic approach for five qubits and more. Figure 3 illustrates the supremacy of this algorithm over the OR-Tools approach.

By a worst-case scenario analysis, it is seen that the time complexity of the algorithm is

$$O(MAX\_ITERATIONS \times p \times d_{max} \times c_{size}),$$
 (10)

where p is the number of observables,  $d_{max}$  is the highest degree of an observable (number of contexts the observable belongs to) and  $c_{size}$  is the highest context size (number of observables in the context, typically three for lines in symplectic spaces). This means that the algorithm has a polynomial complexity, offering a more efficient alternative to the exact methods presented in Section 3.1, which have exponential complexity, for approximating the contextuality degree of quantum configurations.

The convergence speed of our algorithm is depicted in Figure 4, where only the assignment  $min_{-}a$  having the lowest Hamming distance found at each iteration is plotted, hence the decreasing curves.

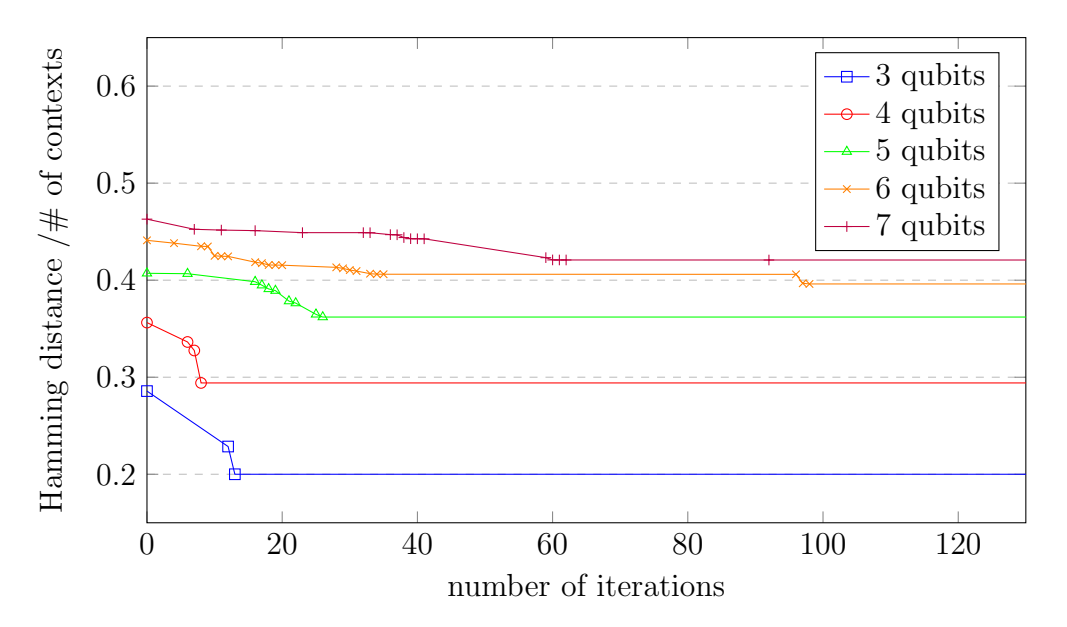


Figure 4: Minimal Hamming distances (the y-axis) per total number of contexts, over the number of iterations (the x-axis), computed by the heuristic method running simultaneously on 200 threads shared between 20 cores of an Intel(R) Core(TM) i7-12700H processor, for the quantum configurations composed of all the lines of the three- to seven-qubit symplectic polar spaces.

### 3.6 Properties of the algorithm as a Markov chain

The algorithm can be formalized as a Markov chain whose transition from the assignment (state) a to the assignment (state) a' obeys the following rule: For any observable o, a'[o] = -a[o] with probability  $\gamma$  if  $uns(a, o) \ge \theta \times \max_{o \in O}(uns(a, o))$  and a[o] otherwise, where uns(a, o) is the number of contexts containing o which are not satisfied by the assignment a and  $\max_{o \in O}(uns(a, o))$  is the maximum of these numbers of unsatisfied contexts among all the observables.

When  $\theta = 0$ , the probability of transition between a and a' is

$$\gamma^{|a'[o] = -a[o]|} \times (1 - \gamma)^{|a'[o] = a[o]|}, \tag{11}$$

where  $|a'[o]| = \pm a[o]|$  denotes the number of observables o satisfying the constraint  $a'[o] = \pm a[o]$ . Provided that  $\gamma \neq 0, 1$ , this probability is strictly positive, meaning that the Markov chain is ergodic; in other words, any arbitrary assignment can be reached after sufficiently many iterations.

However, for  $\theta > 0$ , local minima can trap the algorithm. We demonstrate this with the quantum configuration (O,C) where  $O = \{YIY, XIZ, ZIX, IIY, YII, XXX, ZXZ, ZZZ, XZX\}$  and  $C = \{c_1, \ldots, c_4\}$  with  $c_1 = \{YIY, XIZ, ZIX\}$ ,  $c_2 = \{YIY, IIY, YII\}$ ,  $c_3 = \{YIY, XXX, ZXZ\}$  and  $c_4 = \{YIY, ZZZ, XZX\}$ . The contexts  $c_1$  and  $c_2$  are positive, whereas  $c_3$  and  $c_4$  are negative. When  $\theta > 0.5$  the algorithm starting from the *trivial* assignment (a[o] = 1 for all observables o) only flips one value, namely a[YIY] (with probability  $\gamma$ ), as this observable entails the maximal number of unsatisfied contexts (two, compared to zero or one for the other observables). Then the algorithm either remains in this second state (with probability  $(1 - \gamma)$ ), or returns to the initial trivial assignment. In this orbit of two states the

number of unsatisfied configurations is two, whereas there are assignments satisfying all the context signs, for instance a defined by a[IIY] = a[ZZZ] = -1 and a[o] = 1 for the other observables o. This limitation can be generalized to any  $\theta > 0$  by adding  $1/\theta$  contexts to a counterexample similar to the present one. A variant of the algorithm based on the proportion of unsatisfied contexts among the contexts of each observable also admits similar counterexamples, adding  $1/\theta$  positive contexts to the observables contained only in one context in the counterexample given above.

To sum up, we have shown that the algorithm does not satisfy theoretical properties such as ergodicity (as a Markov chain) and accuracy (the minimum is not always reachable). It indeed belongs to the family of incomplete heuristics. However, these theoretical shortcomings are substantially mitigated by very satisfactory experimental results presented in Sections 3.4 and 3.5, and recast in a geometric language in Section 5.

# 4 Combinatorial geometric estimates of some specific lower bounds

Let  $d_N^{\text{full}}$  be the degree of contextuality for the configuration comprising all the lines/contexts in W(2N-1,2). Generalizing to an arbitrary  $N \geq 3$  the chain of group-geometrical arguments we and Henri de Boutray employed in a previous work [42, Sec. 4.1], we have the following recurrent formula for these degrees

$$d_N^{\text{full}} \ge \frac{\# \text{ of quadratic } \mathcal{W}(2N-3,2)'s \text{ in } \mathcal{W}(2N-1,2)}{\# \text{ of quadratic } \mathcal{W}(2N-3,2)'s \text{ on a line in } \mathcal{W}(2N-1,2)} d_{N-1}^{\text{full}},$$

which, using the combinatorial properties of symplectic polar spaces, can be cast into a simpler form,

$$d_N^{\text{full}} \ge \frac{\text{\# of points in } \mathcal{W}(2N-1,2)}{\text{\# of points in } \mathcal{W}(2N-5,2)} d_{N-1}^{\text{full}},$$

which explicitly reads (see eq. (7))

$$d_N^{\text{full}} \ge \frac{4^N - 1}{4^{N-2} - 1} d_{N-1}^{\text{full}}.$$
(12)

Employing the well-established fact that  $d_2^{\text{full}} = 3$ , we get

$$d_N^{\text{full}} \ge \frac{\left(4^N - 1\right)\left(4^{N-1} - 1\right)}{15}.\tag{13}$$

The values of this lower bound up to nine qubits are as listed in Table 3.

$\overline{N}$	$d_N^{\mathrm{full}} \geq$
2	3
3	63
4	1071
5	17391
6	279279
7	4472559
8	71577327
9	1145302767

Table 3: Lower bound for the degree of contextuality of contextual configurations comprising all the lines of W(2N-1,2) of small rank.

Another set of sufficient (but not necessary) criteria for ascertaining the former lower bound on the contextuality degree of the whole W(2N-1,2), with N>2, is as follows:

$$F_N^{\text{uns}} \cap \mathcal{W}(2N-3,2) \cong F_{N-1}^{\text{uns}} \text{ for any } \mathcal{W}(2N-3,2) \in \mathcal{W}(2N-1,2),$$
 (14)

$$F_N^{\text{uns}} \cap \mathcal{Q}^-(2N-1,2) \cong E_N^{\text{uns}} \text{ for any } \mathcal{Q}^-(2N-1,2) \in \mathcal{W}(2N-1,2)$$
 (15)

and

$$F_N^{\text{uns}} \cap \mathcal{Q}^+(2N-1,2) \cong H_N^{\text{uns}} \text{ for any } \mathcal{Q}^+(2N-1,2) \in \mathcal{W}(2N-1,2).$$
 (16)

In the case of N=3, with the minimal unsatisfied configuration  $F_N^{\text{uns}}\cong\mathcal{H}_C$  and so with  $d_3^{\text{full}}$  reaching its lower bound 63, from the analysis carried out in [42] it follows that all the three criteria are here indeed satisfied. In the next section we will see that this is not the case for N=4.

# 5 Geometries and graphs underpinning the most illustrative four- to six-qubit examples

As it has already been stressed, with the code based on a SAT solver we were unable to properly address contextuality issues for symplectic polar spaces of rank greater than three. To illustrate the power of our new approach, we will discuss in detail the first open case in the hierarchy, N=4, and then briefly address also the N=5 and N=6 cases.

## 5.1 Contextuality in the four-qubit space

#### 5.1.1 Contextuality of elliptic quadrics

A four-qubit elliptic quadric,  $Q^-(7,2)$ , when viewed as a point-line incidence structure, features 119 points and 1071 lines, with 27 lines on a point and three points on a line. The smallest number of negative lines a  $Q^-(7,2)$  can have is 360, which is thus a first upper bound on its contextuality degree  $d_4^{\text{ell}}$ , i. e.,  $d_4^{\text{ell}} \leq 360$ . Using our new approach,

we were able to push this value much lower, namely to  $d_4^{\rm ell} \leq 315$  (see Table 2). The found configuration of 315 unsatisfied contexts,  $E_4^{\rm uns}$ , encompassing all the points of the quadric, features 14 points of degree three (let us call them solids), 21 points of degree seven (dots) and 84 points of degree nine (dashes), as also illustrated in a graphical form in Figure 5, top layer. Out of its 315 lines, there are 21 of type solid-solid-dot, 126 of type dash-dash-dot and, finally, 168 of type dash-dash-dash, as illustrated in Figure 5, bottom layer.

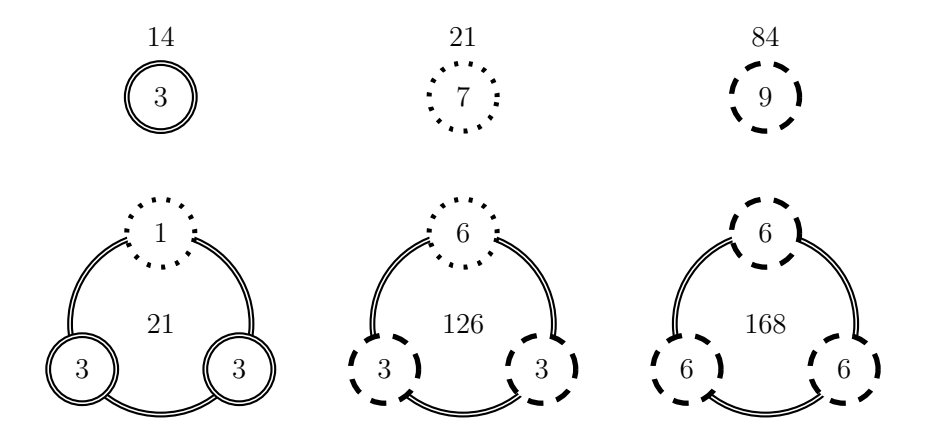
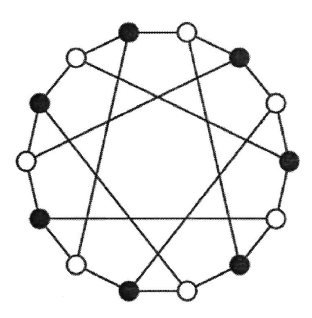


Figure 5: Properties of the point-line geometry comprising 315 unsatisfied constraints of a particular elliptic quadric whose index is *IIIY*. For a point on a line, the number inside the circle corresponds to its restricted degree in the configuration consisting solely of lines of this particular type.

In each line of the first type, the restricted degree of a solid point is three and that of a dotted one is of one. Moreover, the 21 lines of this form can uniquely be associated with the edges of the well-known Heawood graph [13] – see Figure 6, left – in such a way that the 14 solid points will be its vertices and the 21 dotted points will be the third points on its edges so that these edges become lines of W(7,2); hence, this 21-line configuration is isomorphic to nothing but the configuration representing 21 unsatisfied contexts of a three-qubit hyperbolic quadric [30].

Next, let us consider the second configuration of lines. In each of these 126 lines, the restricted degree of a dashed point is three whilst that of a dotted one is six. These 126 lines split into three disjoint, equally-sized sets that are isomorphic to each other. Given such a set, if one considers its 28 dashed points as vertices and the corresponding 42 lines as edges, one obtain a graph that, remarkably, is isomorphic to the famous Coxeter graph [4] – depicted in Figure 6, right. Moreover, joining such a set of 42 'Coxeter' lines<sup>3</sup> with the 21 'Heawood' lines of the first type we get nothing but a copy of the split Cayley hexagon of order two, as schematically depicted in Figure 7 (this being a simplified reproduction of part of Figure 7 of [36]; see also [34,44]). Each of the three split Cayley hexagons is classically embedded into a parabolic quadric  $\mathcal{Q}(6,2)$  in which our elliptic quadric cuts a certain PG(6,2) of the ambient space PG(7,2);

<sup>&</sup>lt;sup>3</sup>It is worth mentioning here that the subgeometry of the split Cayley hexagon of order two related to (or underpinned by) its Coxeter graphs was some 15 years ago found to be intricately related to the  $E_7$ -symmetric black-hole entropy formula in string theory [22].



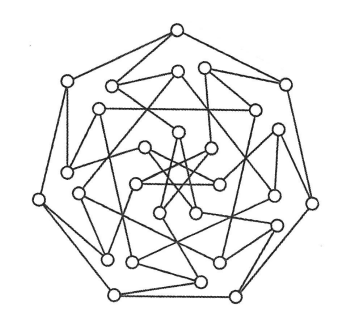


Figure 6: An illustration of the Heawood graph (left) and the Coxeter one (right), both drawn with seven-fold rotational symmetry.

the three corresponding PG(6,2)s have a PG(5,2) in common, the latter cutting our  $Q^-(7,2)$  in a hyperbolic quadric,  $Q^+(5,2)$  – the one accommodating the 14 points of degree three and the 21 points of degree seven. It is worth mentioning here that the 21 points of degree seven form in each hexagon a geometric hyperplane; this smallest-size hyperplane is called a distance-2 ovoid and is of type  $V_2$  in the notation of Frohardt and Johnson [10].

Finally, each of the 168 lines of the last type is such that it shares a single point with each of the three hexagons. Hence, the 12 points located on six lines passing via a dashed point split into two sextuples, either sextuple being located in a hexagon. In addition, each sextuple further splits into a pair of tricentric triads that define a unique quadratic doily.

#### 5.1.2 Contextuality of hyperbolic quadrics

A four-qubit hyperbolic quadric,  $Q^+(7,2)$ , when viewed as a point-line incidence structure, features 135 points and 1575 lines, with 35 lines on a point and three points on a line. The smallest number of negative lines a  $Q^+(7,2)$  can have is 532, hence its degree of contextuality  $d_4^{\text{hyp}}$  satisfies  $d_4^{\text{hyp}} \leq 532$ . As in the preceding case, we can do much better with our new approach, namely  $d_4^{\text{hyp}} \leq 315$  (see Table 2). Here, the pattern of 315 unsatisfied contexts we have discovered,  $H_4^{\text{uns}}$ , that again covers all the points of the quadric, is much more symmetric than that characterizing an elliptic quadric, since through each point here pass the same number of lines, namely seven. Using the Lagrangian Grassmannian mapping of the type LGr(3,6) (see, e.g., [18,21]) that sends planes of  $\mathcal{W}(5,2)$  into points of a certain  $\mathcal{Q}^+(7,2)$  and lines of  $\mathcal{W}(5,2)$  into lines of the same quadric (and whose explicit form we made use of is given in A), this  $(135_7, 315_3)$ -configuration is found to be, in fact, isomorphic to  $\mathcal{DW}(5,2)$ . This is a very important fact in the following sense. We know that each  $Q^+(7,2)$  contains 120 quadratic W(5,2)s. On the other hand,  $\mathcal{D}W(5,2)$  contains the same number of copies of the split Cayley hexagon of order two (these being, in fact, its geometric hyperplanes, see, e.g., [6]). Hence, when a  $\mathcal{DW}(5,2)$  is embedded into a  $\mathcal{Q}^+(7,2)$ , each hexagon must be hosted by a unique  $\mathcal{W}(5,2)$ . In other words, our unsatisfied configuration  $H_4^{\text{uns}}$  picks up from (or shares with) each W(5,2) of the  $Q^+(7,2)$  a single copy of the split Cayley hexagon of order two; moreover, we have verified that it is always a copy that is *classically*-embedded into the corresponding  $\mathcal{W}(5,2)$ . Given the fact that any unsatisfied configuration of the full three-qubit  $\mathcal{W}(5,2)$  is isomorphic

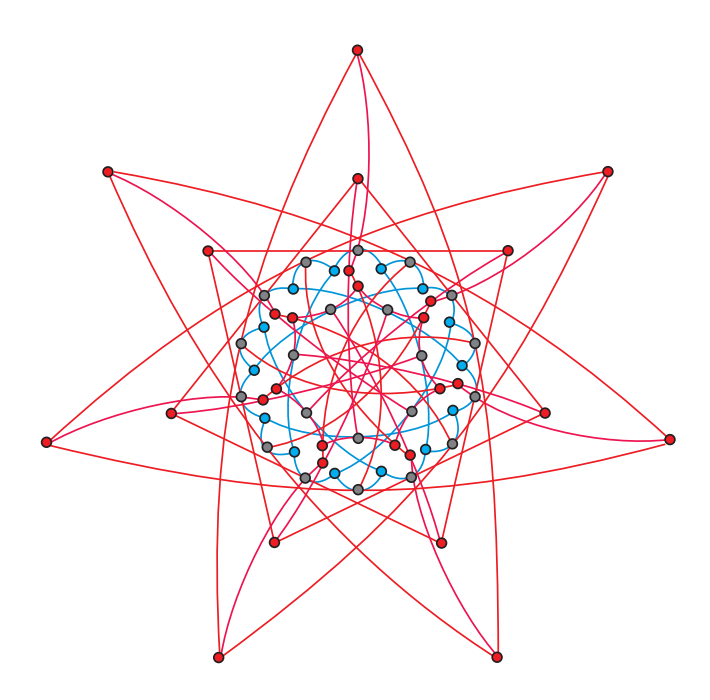


Figure 7: A generic layering of each of the three split Cayley hexagons of order two encapsulating the core of  $E_4^{\rm uns}$ . The 14 solid points are colored blue, the 21 dotted points are gray and 28 out of 84 dashed points are represented by red color. The 21 blue lines are the Heawood lines, those colored red are the Coxeter ones. Removing from the hexagon the 21 gray points we indeed get a disjoint union of the Heawood graph and the Coxeter graph.

to a copy of the smallest split Cayley hexagon embedded classically into the space,  $F_3^{\text{uns}} \cong \mathcal{H}_{\mathcal{C}}$  [30, 42], and a very recent proof [26] that this isomorphism must hold for any  $\mathcal{W}(5,2)$  located in any higher-rank space, our unsatisfied  $H_4^{\text{uns}} \cong \mathcal{DW}(5,2)$  behaves exactly as one would expect for a configuration that also gives the *lower* bound for the contextuality degree of the four-qubit  $\mathcal{Q}^+(7,2)$ . Moreover, we have also verified that both  $\mathcal{DW}(5,2)$  and its complement on the  $\mathcal{Q}^+(7,2)$  are, like an  $\mathcal{H}_{\mathcal{C}}$  and its complement in  $\mathcal{W}(5,2)$ , not contextual. There is also a neat combinatorial argument speaking in favor of our conjecture. There are altogether 136  $\mathcal{Q}^+(7,2)$ 's in  $\mathcal{W}(7,2)$ , each of them has 1575 lines and as there are 5355 lines in  $\mathcal{W}(7,2)$ , each line of this space is shared by  $136 \times 1575/5355 = 40 \mathcal{Q}^+(7,2)$ 's. And, remarkably,  $136 \times 315/40 = 1071$ , which is indeed equal to the lower bound ascertained in Section 4 (see Table 3) for the degree of contextuality of the configuration comprising all the lines of  $\mathcal{W}(7,2)$ . So, we do believe that  $d_4^{\text{hyp}} = 315$ , with the understanding that the corresponding unsatisfied configurations are (always) isomorphic to  $\mathcal{DW}(5,2)$ .

#### 5.1.3 Contextuality of the full four-qubit space

The full four-qubit space, W(7,2), features 255 points and 5 355 lines, with 63 lines through a point and three points on a line. As 1 908 out of its 5 355 contexts are negative,  $d_4^{\text{full}} \leq 1908$ . Also this bound has been considerably reduced, down to 1 575 (see Table 1). This bound is also the number of lines on a  $Q^+(7,2)$  – an intrigu-

ing coincidence. The corresponding configuration of 1575 unsatisfied contexts,  $F_4^{\rm uns}$ , encompassing all the 255 points of the space, features 30 points of degree seven (to be referred to as solids), 105 points of degree 19 (dots) and 120 points of degree 21 (dashes), as also illustrated in a graphical form in Figure 8, top layer. Out of its 1575 lines, there are 105 of type solid-solid-dot, 210 of type dot-dot-dot and, finally, 1260 of type dash-dash-dot, as illustrated in Figure 8, bottom layer.

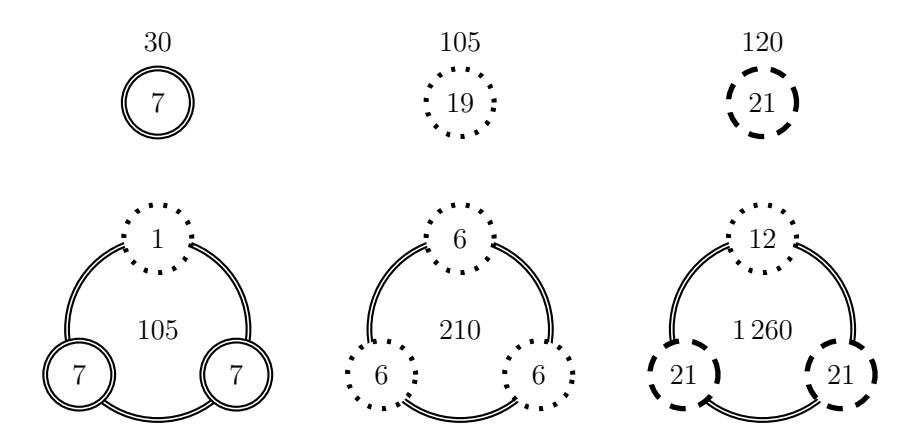


Figure 8: Properties of the point-line geometry comprising 1575 unsatisfied constraints for the contextual geometry whose contexts are all the lines of the space W(7, 2).

In each line of the first type, the restricted degree of a solid point is seven and that of a dotted one is of one. The 105 lines of this form can uniquely be associated with the edges of the point-plane incidence graph of PG(3,2) in such a way that the 30 solid points will be its vertices and the 105 dotted points will be the third points on its edges so that these edges become lines of W(7,2) – as also illustrated in Figure 9. Moreover, these lines together with the 210 lines of the second type form a geometry isomorphic to  $\mathcal{D}W(5,2)$ , which is fully located on a particular hyperbolic quadric that consists of the 30 points of degree seven and the 105 points of order 19 (and whose index, as readily discernible from Figure 9, is XYYZ). Interestingly, the 105 points of order 19 form in the  $\mathcal{D}W(5,2)$  a geometric hyperplane, namely the one belonging to class 3 in the classification of Pralle [37].

Using our Haar-graph-based geometry of Figure 9, the 210 lines of the second type are found to form 13 orbits of size 15 and three orbits of size five with respect to the action of the automorphism of order 15 of the figure. A representative line for each of these orbits is portrayed in Figure 10. In particular, we have for the encircled-filled part the lines YYXI-YXYI-IZZI (blue), XZZI-IZZY-XIIY (green), YZYI-IZYY-YIIY (red), XXXZ-XXXI-IIIZ (yellow) and YZZY-ZXII-XYZY (violet); for the plain-filled family the lines IYZZ-IXYZ-IZXI (blue), XZXY-ZXYX-YYZZ (red), YYXY-ZIIX-XYXZ (yellow) and ZIYI-YZXZ-XZZZ (violet); and for the circled color set the lines YIXX-YYYZ-IYZY (blue), IXYY-IXZZ-IIXX (green), YZIX-YXYY-IYYZ (yellow) and IYYI-IIIY-IYYY (violet). The three representatives of size-five orbits are: IYZI-YIII-YYZI (squares), YXZZ-XYXY-ZZYX (diamonds) and IZXZ-YIIZ-YZXI (triangles).

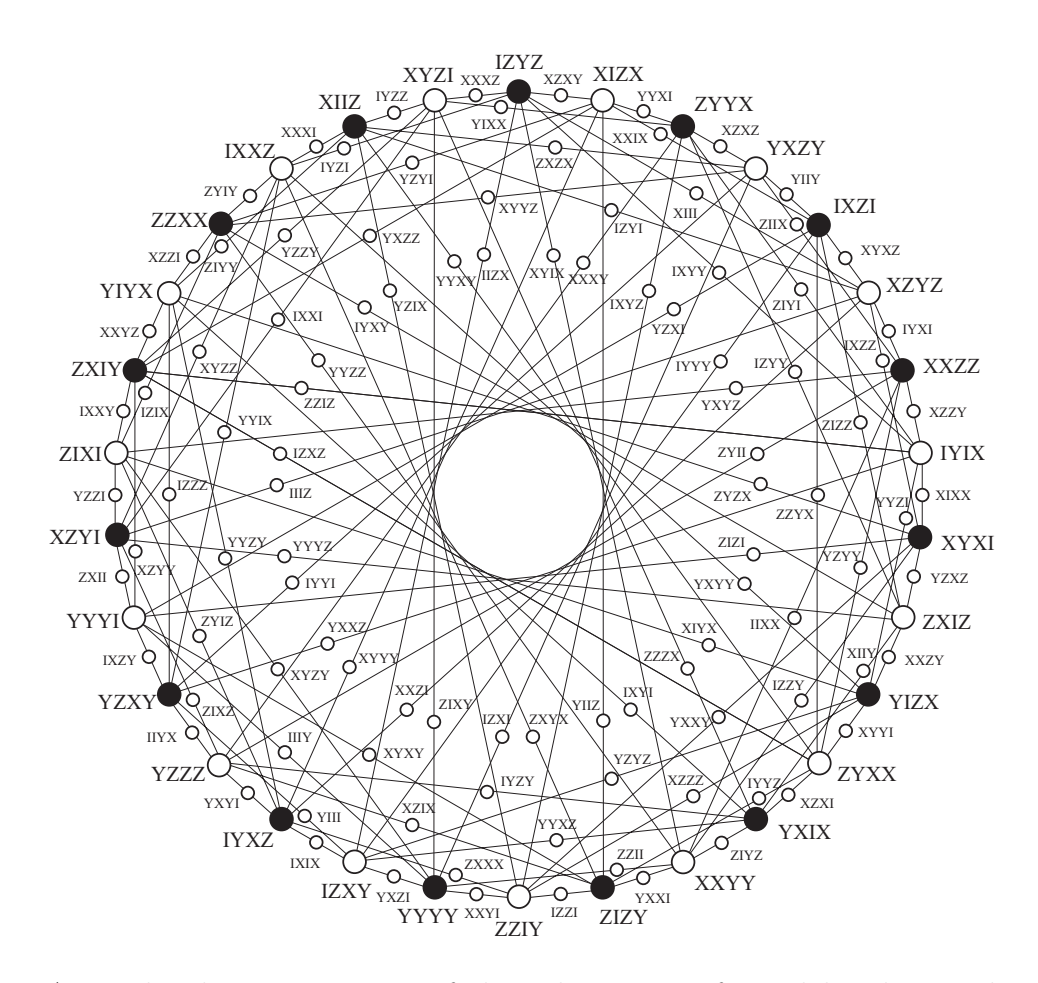


Figure 9: A graphical representation of the subgeometry formed by the 105 lines of the first type. The underlying point-plane incidence graph of PG(3,2) – whose vertices are represented by 15 big white circles as well as 15 big black circles (bullets) – is rendered in the rotationally symmetric form isomorphic to the Haar graph H(17051).

Let us, finally, focus on the dash-type points and the lines of the last, i.e. dashdash-dot type. The 120 dash-type points are exactly those points that lie out off the hyperbolic quadric  $\mathcal{Q}_{XYYZ}^+(7,2)$  that hosts our unsatisfied  $\mathcal{DW}(5,2)$ . Through each of these points there pass 21 lines of the above-mentioned type that cut the  $Q_{XYYZ}^+(7,2)$  in the 21 points of the dot-type. By a way of example, the 21 lines through the (off-quadric) point IIYI cut the  $Q_{XYYZ}^+(7,2)$  in the 21 points shown in Figure 11 in gray color. Each of these points is incident with a unique line of the first type (bold gray) whose other two points are the vertices of the point-plane incidence graph of PG(3,2), illustrated in Figure 11 by big gray circles. There are 14 such vertices that together with 21 distinguished edges form a subgraph of the point-plane incidence graph of PG(3,2) that is isomorphic to the Heawood graph. The 35 points of this Heawood-graph-underpinned geometry define a certain  $\mathcal{Q}^+(5,2)$  in some PG(5,2) of the ambient PG(7,2). Our selected point IIYI is also the nucleus of a unique quadratic  $\widetilde{\mathcal{W}}(5,2) \in \mathcal{Q}^+_{XYYZ}(7,2)$  that contains  $\widetilde{\mathcal{Q}}^+(5,2)$ ; the 28 points of  $\widetilde{\mathcal{W}}(5,2)$  that lie off  $\widetilde{\mathcal{Q}}^+(5,2)$  are show in Figure 11 by yellow color. Next, there exists a unique elliptic quadric,  $\widetilde{\mathcal{Q}}^-(7,2) \in \mathcal{W}(7,2)$  that shares with  $\mathcal{Q}^+_{XYYZ}(7,2)$  our  $\widetilde{\mathcal{W}}(5,2)$ .

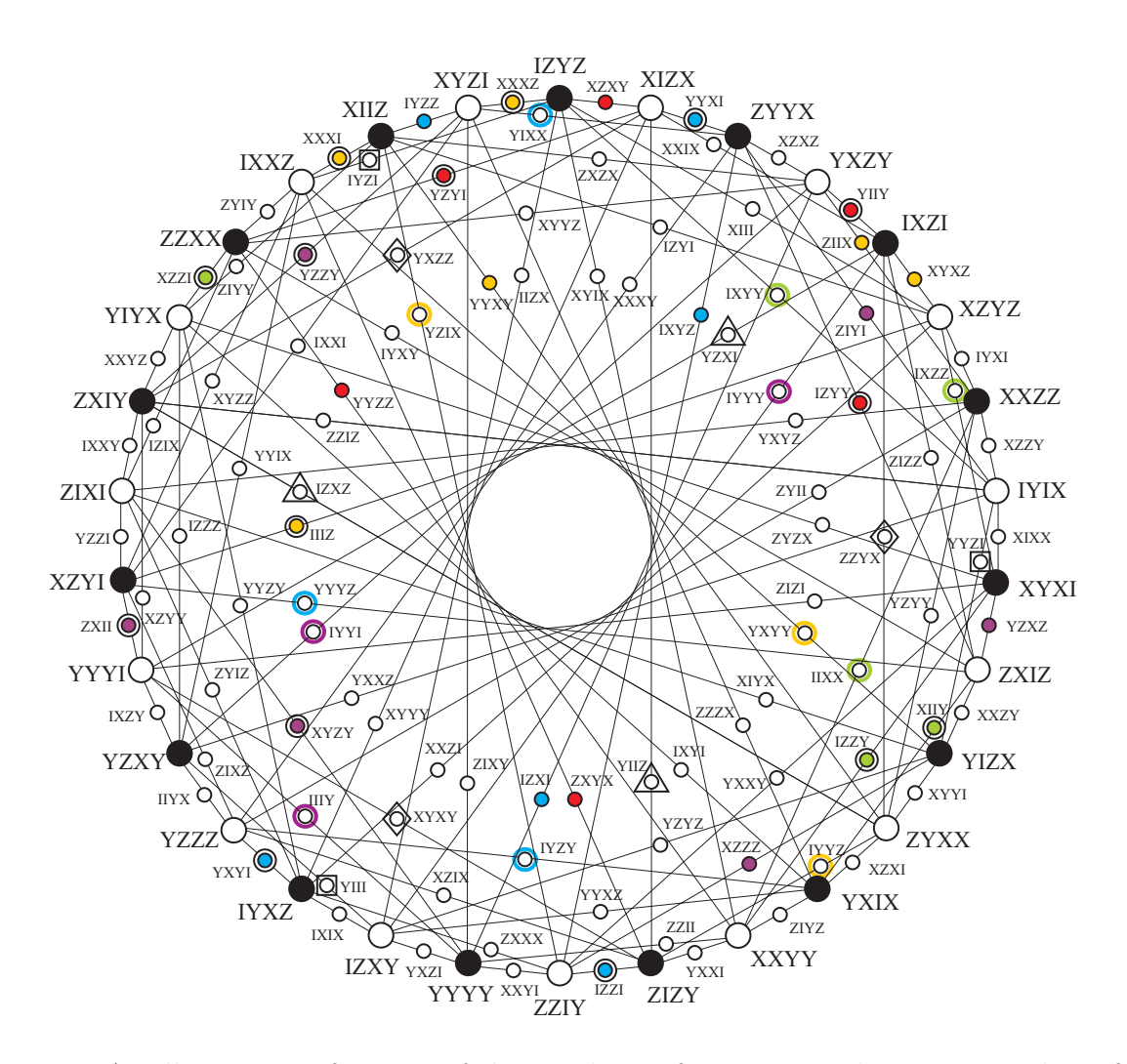


Figure 10: An illustration of 16 out of the 210 lines of type two. The remaining lines from each orbit can be obtained by successive rotations of the figure through 360/15 degrees around its center while keeping the position of each label/observable fixed.

Its remaining (119 – 63 =) 56 points can be found as follows. We consider the (non-isotropic) line that is polar to the above-defined PG(5, 2) with respect to the symplectic polarity defining W(7,2). This line passes, obviously, through the point IIYI and its remaining two points are found among the vertices of our point-plane incidence graph of PG(3, 2) – as also illustrated in Figure 11. One of them is XYZI (green), which is exactly the vertex connected to those seven vertices of the Heawood (sub-)graph that are represented by bullets, whereas the other one, XYXI (blue), is that vertex that is connected to the other set of seven vertices, represented by big circles. As neither of the two points lies on the  $\widetilde{Q}^-(7,2)$ , they are the nuclei of two different quadratic W(5,2)' and W(5,2)'' lying on  $\widetilde{Q}^-(7,2)$  and having  $\widetilde{Q}^+(5,2)$  in common; our remaining 56 points of  $\widetilde{Q}^-(7,2)$  are nothing but those 56 points (of dash type) that belong to the symmetric difference of W(5,2)' and W(5,2)''. It is a straightforward, though by hand a bit lengthy, task to verify that  $F_4^{\text{uns}}$  shares with both W(5,2)' and W(5,2)'', like with  $\widetilde{W}(5,2)$  itself, a (classically-embedded) copy of the split Cayley hexagon of

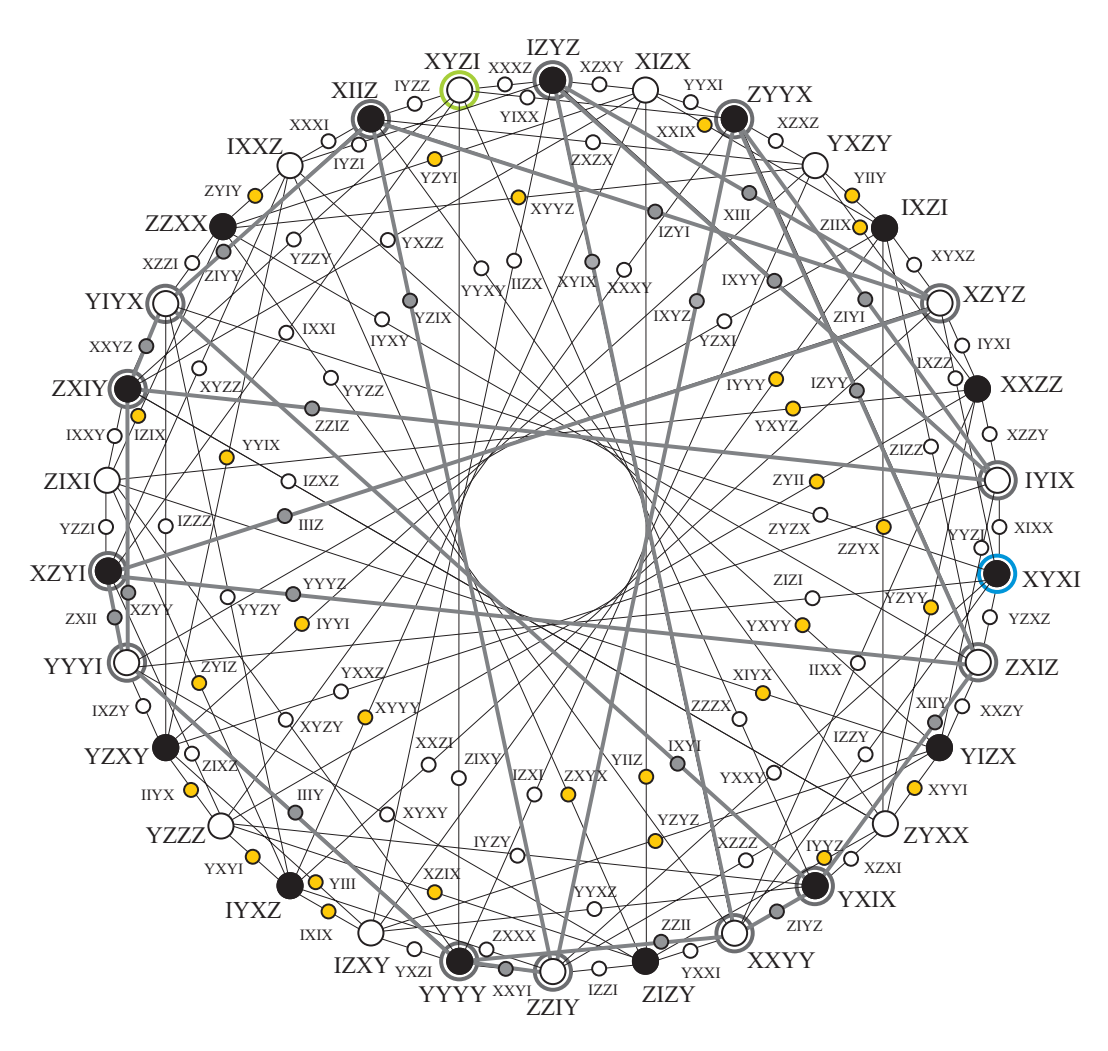


Figure 11: An illustration of main properties of the points and lines of the third type. The meaning of the colored points and highlighted lines is described in the text.

order two, the three hexagons having the above-described Heawood-graph-underpinned configuration in common. And this property holds if we take instead IIYI any other point of the dash type.

Obviously, reversing the above-given chain of reasoning helps us find all 1 260 lines of the third type solely from the configuration formed by the 105 type-one lines, once the latter are represented as portrayed in Figure 9. A specific case of this reversed procedure is portrayed in Figure 12. Let us start with Figure 9. In its underlying point-plane incidence graph of PG(3,2), let us pick up an arbitrary black vertex,  $\mathcal{O}_f$ , and an arbitrary white vertex not adjacent to it,  $\mathcal{O}_e$ ; the third point on the line defined by the two vertices,  $\mathcal{O}_f.\mathcal{O}_e$ , lies clearly off the quadric  $\mathcal{Q}_{XYYZ}^+(7,2)$  because the two corresponding observables anti-commute (and so the line does not belong to  $\mathcal{W}(7,2)$  and, hence, to  $\mathcal{Q}_{XYYZ}^+(7,2)$ ). Next, take all the seven white vertices adjacent to  $\mathcal{O}_f$  as well as all the seven black ones adjacent to  $\mathcal{O}_e$ ; these 14 vertices together with the corresponding 21 edges inherited from the point-plane incidence graph of PG(3,2) form a graph that is isomorphic to the Heawood graph. Connecting the point  $\mathcal{O}_f.\mathcal{O}_e$  with each of the 21 mid-points situated on the edges of this Heawood graph one gets

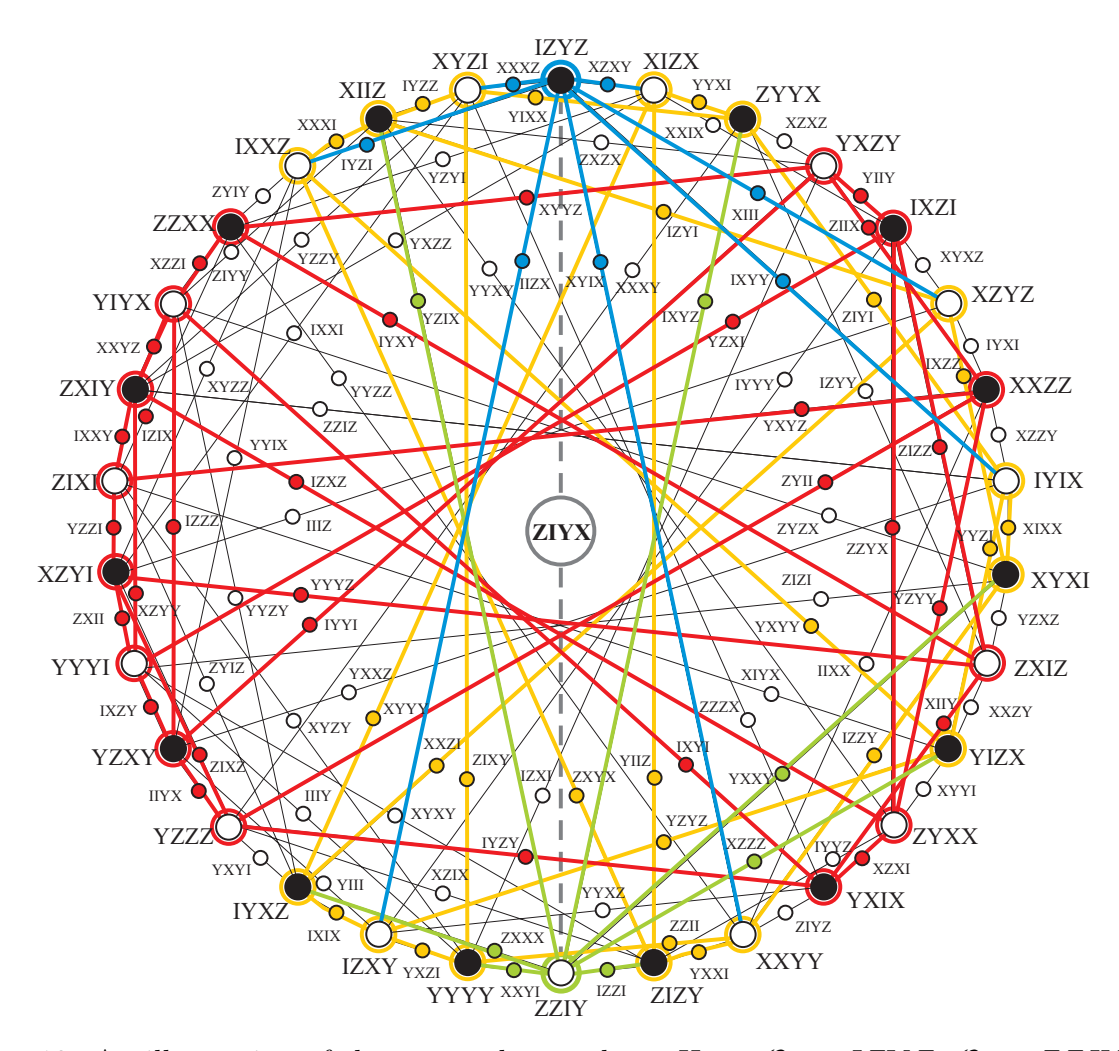


Figure 12: An illustration of the reversed procedure. Here,  $\mathcal{O}_f = IZYZ$ ,  $\mathcal{O}_e = ZZIY$  and  $\mathcal{O}_f.\mathcal{O}_e = ZIYX$ . The seven neighbors of  $\mathcal{O}_f$  are pointed out by blue edges, those of  $\mathcal{O}_e$  by green ones and the associated Heawood graph is highlighted in yellow color. (Interestingly, the complement of the Heawood graph, that is the quartic bipartite graph on 14 vertices and 28 edges highlighted in red color, is nothing but the Levi graph of the biplane of order two.)

all the 21 lines of type three passing via this particular off-quadric point. Now, since there are  $15 \times (15-7) = 120$  black-white vertex pairs of the above-defined type and no two such pairs define the same off-quadric point (otherwise the corresponding four vertices would be coplanar, which is impossible), this construction yields indeed all  $120 \times 21/2 = 1260$  lines of the dash-dash-dot type.

At this point, it is particularly instructive to make a slight digression from the main course of the paper and show that the just-outlined reversed procedure yields in the three-qubit case a copy of the split Cayley hexagon of order two, i. e.,  $F_3^{\text{uns}}$ , and in the two-qubit doily just three pairwise disjoint lines, i. e.,  $F_2^{\text{uns}}$ . The three-qubit analogue of  $\mathcal{DW}(5,2)$  is a Heawood-graph-underpinned configuration [30,42] featuring 35 points and 21 lines, which can be taken – without any substantial loss of generality – to be located on the symmetric hyperbolic quadric,  $\mathcal{Q}_{III}^+(5,2)$ , as portrayed in Figure 13. From the underlying Heawood graph we pick up an arbitrary white vertex, say XXI

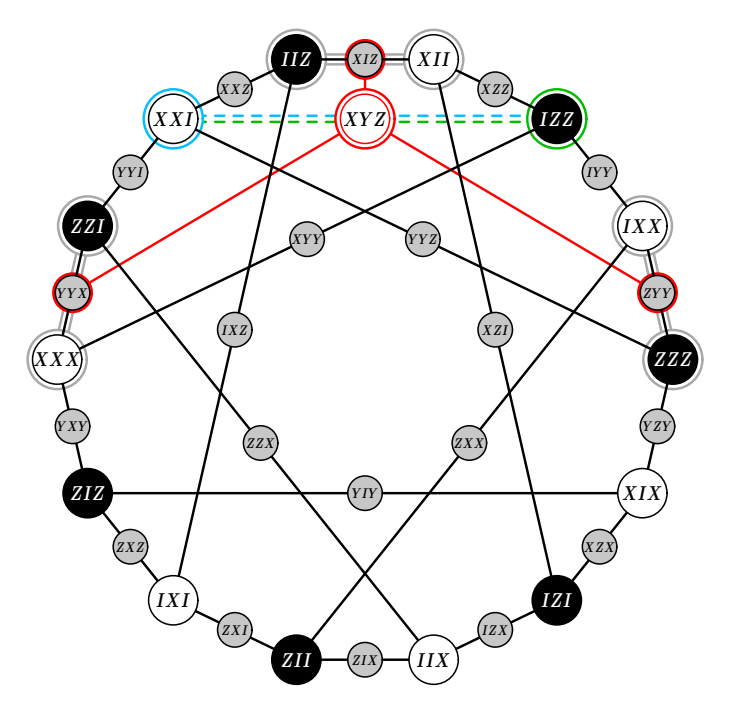


Figure 13: An illustration showing how, starting with the Heawood-graph-underpinned configuration in the three-qubit polar space, W(5,2), we can get the remaining 28 points and 42 lines of a classically-embedded copy of the split Cayley hexagon of order two. The role of color-highlighted elements is explained in the main text.

(blue), and any black one that is not adjacent to it, say IZZ (green). The two vertices define a non-isotropic line of the ambient PG(5,2) (dashed blue-green) whose third point, XYZ (red), is skew-symmetric and thus lies off the quadric. Let us consider, in analogy with the four-qubit case, the graph consisting of the three black vertices that are adjacent to XXI (encircled gray), the three white vertices adjacent to IZZ (also encircled gray) and the corresponding three inherited edges (gray parallel segments) – which is the graph isomorphic to the Haar graph H(4) (or, equivalently, to the pointpoint incidence graph of PG(1,2)). Joining the 'red' point XYZ with each of the three mid-points lying on the edges of the H(4) we get three out of 42 off-quadric lines of the hexagon (illustrated without third points by red segments). As there are  $7\times(7-3)=28$  black-white vertex pairs of the above-defined type and no two such pairs define the same off-quadric point, repeating this procedure we get all 28 off-quadric points of the hexagon and  $28 \times 3/2 = 42$  remaining lines of the hexagon. It is also obvious that three lines issued from each 'red' point lie in the same plane of  $\mathcal{W}(5,2)$ , which means (see, e.g., [42]) that a copy of the split Cayley hexagon we get by this construction is indeed classically embedded into W(5,2).

In the two-qubit case, our starting point is a configuration isomorphic to the above-introduced H(4)-graph-underpinned configuration. This configuration comprises three pairwise disjoint lines of the doily and lies on one of its hyperbolic quadrics, which is again taken to be the symmetric one,  $Q_{II}^+(3,2)$  – as sketched in Figure 14. As before, let us consider two non-adjacent vertices of the underlying H(4) graph, one white (e. g. IX (green)) and one black (e. g. IZ (blue)). They define an off-doily line (double dashed) whose third point (IY (red)) lies off the quadric. It is obvious that here we

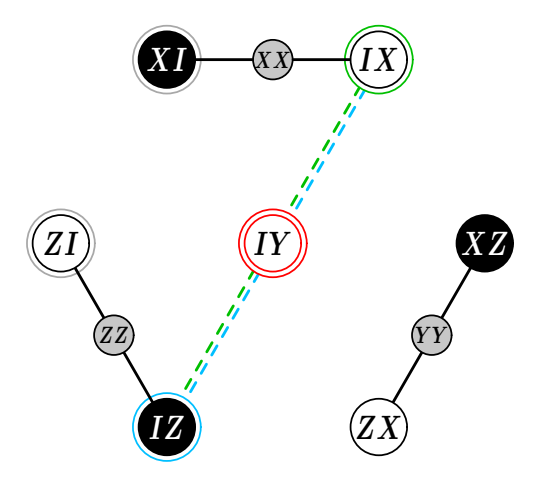


Figure 14: An illustration demonstrating that given a point-hyperplane incidence graph of PG(1,2) embedded into the two-qubit symplectic polar space, our procedure does not result in any other 'red' line of the space. (Compare with Figure 13.)

have only two different points that are adjacent to our selected points; namely, XI (neighbor to IX) and ZI (adjacent to IZ). Since these two vertices are not adjacent our procedure, in contrast with the above discussed two cases, ends here, thus not yielding any further line of the doily passing through the 'red' point IY! And since the absence of 'red' lines characterizes any off-quadric point in the doily, this finding can be rephrased by saying that a set of three lines of the doily associated with the three edges of an H(4) graph will always be the only unsatisfied contexts for the contextual configuration comprising all the 15 contexts of the two-qubit doily. This also provides a sort of explanation for the fact that  $F_2^{\rm uns}$  does not cover all the points of the doily.

To conclude this subsection we return back to the central theme by stressing the following striking observation: whereas  $F_4^{\text{uns}} \cap \mathcal{Q}^-(7,2) \cong E_4^{\text{uns}}$  for any  $\mathcal{Q}^-(7,2) \in \mathcal{W}(7,2)$  (that is to say, criterion (15) is satisfied),  $F_4^{\text{uns}} \cap \mathcal{Q}^+(7,2) \cong H_4^{\text{uns}}$  holds just for a single  $\mathcal{Q}^+(7,2) \in \mathcal{W}(7,2)$  (and so criterion (16) does not hold)!

## 5.2 Contextuality in the five-qubit space

The complexity of unsatisfied configurations we found here is much greater than in the previous case and so we will only describe their basic features.

We will start with hyperbolic quadrics. Such a quadric,  $Q^+(9,2)$ , features 527 points and 23 715 lines of which no less than 9 420 can be negative. A related unsatisfied configuration we found contains only 6 975 lines, so  $d_5^{\text{hyp}} \leq 6\,975$  (see Table 2). This configuration exhibits a very high degree of symmetry as it has only two kinds of points and, similarly, two types of lines. Out of the 527 points, 62 are of degree 15 (solids) and 465 of degree 43 (dashes). Out of the 6 975 lines, there are 465 of type solid-solid-dash and the remaining 6 510 ones are of type dash-dash-dash. Remarkably, one can associate the 62 solid points with the 62 vertices of the point-hyperplane incidence graph of PG(4, 2) in such a way that the 465 lines of the former type will be represented by the edges of this graph – as illustrated in Figure 15. If we compare this result with what we found for the four-qubit hyperbolic quadrics (see Figure 9) and for three-qubit ones (see Figure 2 in [30]), we arrive at the following natural conjecture: the

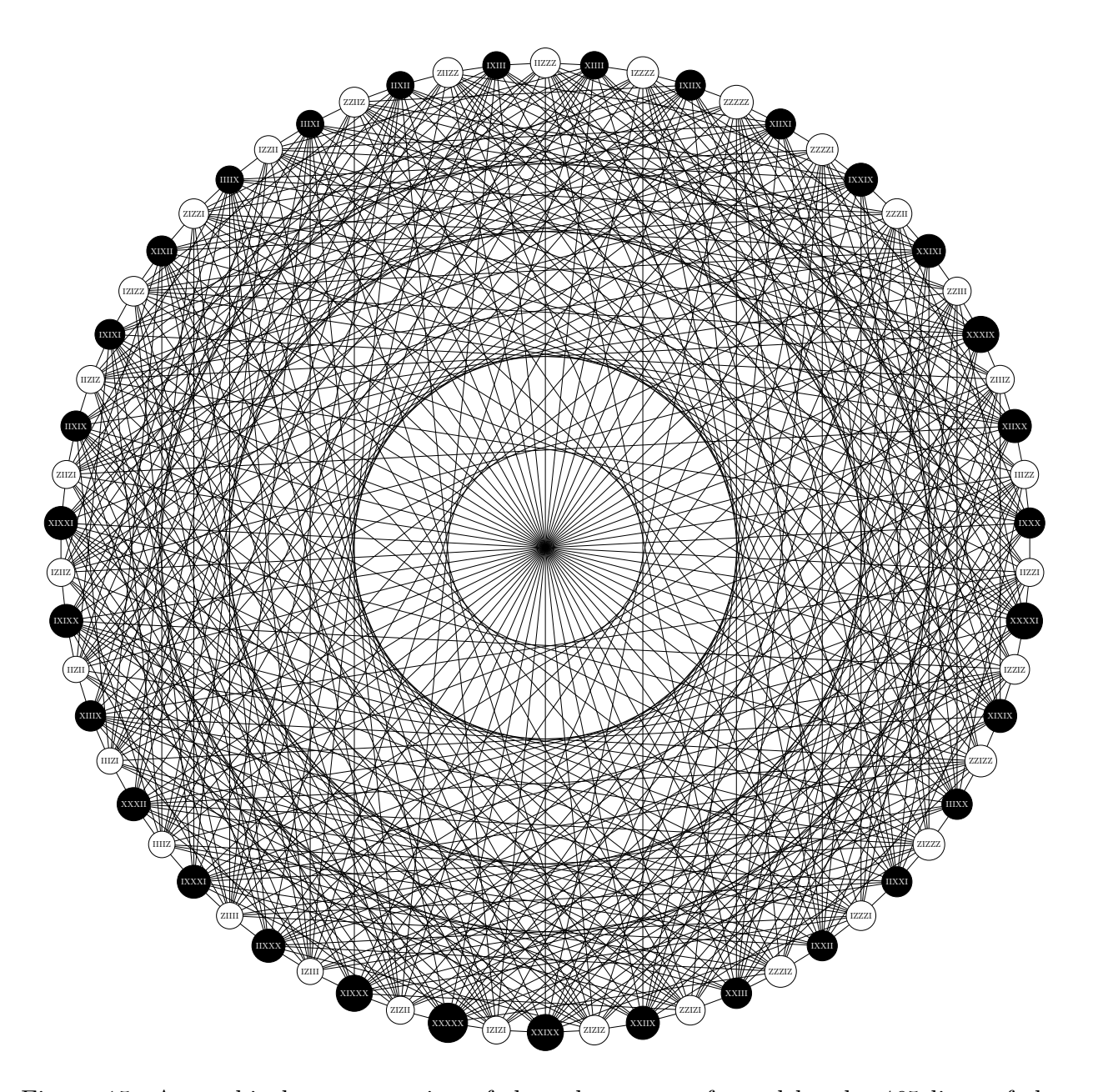


Figure 15: A graphical representation of the subgeometry formed by the 465 lines of the first type; in order not to make the figure to look much too crowded, the 465 points of the dash type are not shown. The underlying point-hyperplane incidence graph of PG(4,2) is rendered in the form isomorphic to the Haar graph H(1103671145) whose number was computed for us by Dr. Eric W. Weisstein (Wolfram Research).

core geometry of an unsatisfied configuration of a hyperbolic quadric  $Q^+(2N-1,2)$ ,  $N \geq 3$ , is underlined by the point-hyperplane incidence graph of the projective space PG(N-1,2).

An elliptic quadric,  $Q^-(9,2)$ , is endowed with 495 points and 19 635 lines, of which no less than 7 860 can be negative. An upper bound we found in this case, for  $d_5^{\text{ell}}$ , amounts to 7 087 (see Table 2). The corresponding configuration is already too complex to be described in sufficient detail. We only mention that its points are of as many as 11 different degrees, all odd, the smallest being seven and the largest 51, with only two points being of the smallest degree.

In the case of the contextual configuration comprising all 86 955 lines of the five-qubit space W(9,2), we found an unsatisfied configuration having 31 479 lines ( $d_5^{\text{full}} \leq 31479$ , see Table 1), which is less than 35 400, the number of negative lines in this space. Among its points, we find again 11 distinct degrees, the smallest being 15 and the largest one amounting to 105. Strikingly, among cardinalities of different degrees we spot some distinguished numbers that occur in the three-qubit space. In particular, there are two sets of points of different degree having 288 elements either, which could be related to 288 Conwell heptads of W(5,2) [41]. Further, there are 105 points of degree 99, this pointing out to the 105 lines located on a  $Q^+(5,2)$ . These and several other intriguing observations will be treated in a separate paper.

### 5.3 Contextuality in the six-qubit space

To round off our exposition of illustrative examples, we will also briefly address the six-qubit space.

Here, our unsatisfied geometry associated with the contextual configuration comprising all 1 396 395 lines of  $\mathcal{W}(11,2)$  exhibits a great degree of combinatorial simplicity as it has only two different types of points and three distinct types of lines. In particular, out of the 4095 points of  $\mathcal{W}(11,2)$ , there are 126 of degree 192 (solids) and 3 969 of degree 412 (dots), as portrayed in Figure 16, top layer. The totality of 553 140 ( $d_0^{\text{full}} \leq 553\,140$ , much smaller than 615 888, the total number of negative contexts) unsatisfied lines features 126 lines of type solid-solid-solid, 23 814 lines of type solid-dot-dot and the remaining 529 200 ones consisting solely of dots – see Figure 16, bottom layer. The 126 lines of the first type are quite interesting as they split into two equally-sized disjoint sets, either of the two sets being isomorphic to nothing but a copy of the split Cayley hexagon of order two classically embedded into the subspace  $\mathcal{W}(5,2)$  it spans, i. e., to an  $F_3^{\text{uns}}$ .

In the unsatisfied configuration associated with a hyperbolic quadric of the space we find as many as five different types of points and eight types of lines. Among its 2079 points, there are 14 of the smallest degree (31) and 49 of the largest one (211); moreover, the number of points having one specific degree (155) is equal to the number of linear doilies in W(5,2) - 336 [41]. Among its 132 391 lines ( $d_6^{\text{hyp}} \leq 132 391$ , see Table 2), there is a particular type of size 49 whose elements can be associated with the edges of the complete bipartite graph  $K_{7,7}$  (aka the adjacency graph of the Fano plane)<sup>4</sup>; each such line consists of two points of the smallest degree and one point of the largest one.

<sup>&</sup>lt;sup>4</sup>We note in passing that the Heawood graph is a subgraph of the  $K_{7,7}$ -graph.

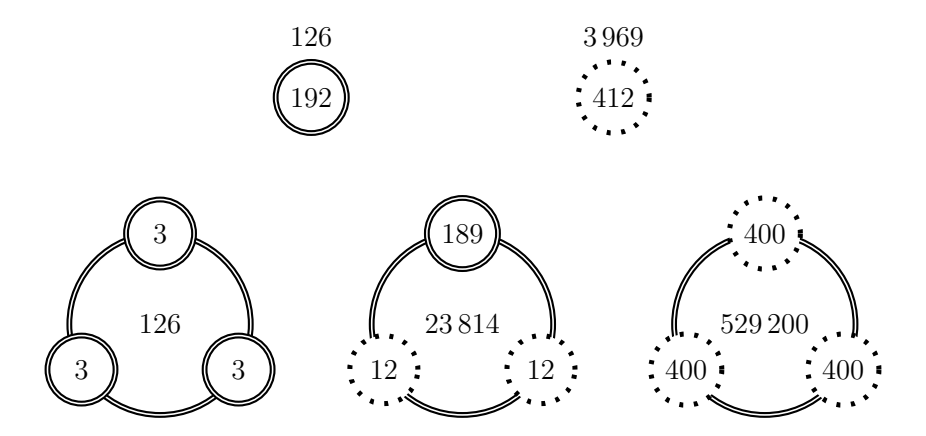


Figure 16: Properties of the point-line geometry comprising 553 140 unsatisfied constraints for the contextual geometry whose contexts are all the lines of the space W(11, 2), following the notation set up in Figure 5.

Finally, the unsatisfied configuration we found for an elliptic quadric, comprising 131 700 lines ( $d_6^{\rm ell} \leq 131\,700$ , see Table 2), is the most complex of the three. The 2015 points of the quadric split into six different types and it is instructive to list them explicitly: 14 points of degree 84, 27 points of degree 92, 21 points of degree 100, 378 points of degree 196, 1008 points of degree 198 and 567 points of degree 204. The 27 points of degree 92 are found to be located on nine pairwise disjoint lines and so form a configuration isomorphic to  $E_3^{\rm uns}$ . Moreover, the 14 points of degree 84 together with 21 points of degree 100 are situated on 21 lines that can be associated with the edges of the Heawood graph and so they form the configuration isomorphic to  $H_3^{\rm uns}$ . Finally, it is worth noticing that the number of points of degree 198 is the same as that of quadratic doilies living in  $\mathcal{W}(5,2)$  [41], or as the number of ordinary hexagons contained in the split Cayley hexagon of order two.

## 6 Discussion

Making use of a new heuristic method in combination with symmetries exhibited by (specific subgeometries of) the multi-qubit symplectic polar space of order two  $\mathcal{W}(2N-1,2)$ , we were able, for  $4 \leq N \leq 7$  qubits, to push the upper bounds on the degree of contextuality of contextual configurations living in  $\mathcal{W}(2N-1,2)$  much lower than those found with the previous method based on a SAT solver, and than the smallest number of negative lines a configuration of a given type can be endowed with. The power of this method is best illustrated with the four-qubit case, where we also achieved a deep, and fairly detailed, insight into the nature of those parts of contextual configurations that are irreproducible by any NCHV model. The corresponding unsatisfied part of an elliptic quadric has in its core three copies of the split Cayley hexagon of order two sharing the Heawood graph and covering all the points of the quadric; this is quite an important finding in light of the fact that the split Cayley hexagon of order two is the geometry that rules contextuality in the three-qubit  $\mathcal{W}(5,2)$  [42]. The unsatisfied contexts of a hyperbolic quadric are arranged into a structure isomorphic

to  $\mathcal{DW}(5,2)$ , the space that is dual to  $\mathcal{W}(5,2)$ ; here, we surmise to have reached also the lower bound. Interestingly, an unsatisfied copy of  $\mathcal{DW}(5,2)$  also occurs in the case when all the lines of  $\mathcal{W}(7,2)$  are considered as a contextual configuration, this time centered on a distinguished point-plane incidence graph of PG(3,2) and surrounded by additional 1260 unsatisfied contexts. Hence, in all the three cases we see a clear connection with the three-qubit symplectic polar space  $\mathcal{W}(5,2)$ . Another intriguing fact in the four-qubit space is that two identical upper bounds (315) correspond to contextual configurations that are geometrically very different. Moreover, the upper bound we found for the contextuality degree of the whole space (1575) coincides with the number of lines on a hyperbolic quadric. Also, in the case of hyperbolic quadrics of three-, four- and five-qubit spaces we see an intriguing pattern where the core parts of the corresponding unsatisfied configurations are underpinned by the point-hyperplane incidence graphs of PG(d,2), with d=2,3 and 4, respectively.

Apart from dissecting in a similar fashion some higher-rank cases, we also plan to employ our new method to deal with contextual configurations whose contexts have more than three observables. For example, a natural context with four elements is isomorphic to an affine plane of order two, AG(2,2). In  $\mathcal{W}(5,2)$ , there are already as many as 945 of them and it would be desirable to see what kind of contextual configurations they form, what the corresponding unsatisfied parts of them look like and how these are related to three-element-context configurations in this space. A well-known example of such a configuration is the so-called Mermin pentagram [24]. There are 12 096 distinct pentagrams in W(5,2) and their properties have already been thoroughly analyzed [23, 33, 40]. We would like to perform a similar study for other AG(2,2)-based classes of contextual configurations living in  $\mathcal{W}(5,2)$ . The largest of them is the  $(63_{60}, 945_4)$ -configuration that consists of all 945 AG(2, 2)'s and its degree of contextuality should be equal to 189. We can arrive at this number in two different ways. One of them employs properties of the above-mentioned Mermin pentagrams. Thus, as each AG(2,2) is contained in  $12\,096 \times 5/945 = 64$  such pentagrams and the degree of contextuality of each pentagram is equal to one, we indeed get  $12\,096 \times 1/64 =$ 189. The other one makes use of the configuration comprising all 315 lines of  $\mathcal{W}(5,2)$ , whose degree of contextuality amounts to 63 [30]. Now, there are three planes through a line in  $\mathcal{W}(5,2)$  and, so, there are three distinguished AG(2,2)s that we get by removing this common line from each of the three planes. Hence, it is natural to assume that to each of the 63 unsatisfied line contexts there will be three unsatisfied affine ones, which again yields  $63 \times 3 = 189$ .

Another interesting task would be to explore those contextual configurations that are common to two (or more) different W(2N-1,2)'s living in the same ambient space PG(2N-1,2). The total number of (non-degenerate) symplectic polarities of rank N in PG(2N-1,2),  $S_N$ , is given by the following formula (see, e.g., [8], page 46)

$$S_N = 2^{((2N-1)^2-1)/4} \prod_{i=1}^{N-1} (2^{2i+1}-1).$$

Thus, we find that there are  $S_2 = 2^2(2^3 - 1) = 28$  distinct doilies in PG(3,2). The set of lines shared by two different doilies is usually referred to as a *linear congruence*. Such a congruence is rather simple, comprising either a set of five pairwise disjoint lines forming a spread of PG(3,2) (called an *elliptic congruence*), or a set of six lines lying in pairs in three planes meeting a distinguished line, the latter inclusive (a *parabolic* 

congruence;<sup>5</sup> see, e.g., [14, Section 15.2] or [9, §§ 8–17]. However, in PG(5,2) we already find as many as  $S_3 = 2^6(2^3 - 1)(2^5 - 1) = 64 \times 7 \times 31 = 13\,888$  distinct  $\mathcal{W}(5,2)$ 's and so we expect a greater variety and complexity of intersection patterns, which can still be tractable by our new method. On the other hand, we can – for some small values of N > 2 – consider all elliptic and hyperbolic quadrics contained in PG(2N - 1, 2) and check quantum contextuality of their individual intersections with some selected  $\mathcal{W}(2N - 1, 2)$  of the space.

Finally, there is, as aptly pointed out by one of the reviewers, one more important aspect of our approach to be addressed, namely the fact how the geometric combinatorial properties of sub-geometries of  $\mathcal{W}(2N-1,2)$  so to say "affect" the contextuality results and their accuracy. As already stressed throughout the text, finding the degree of contextuality of a particular (sub-)geometry amounts to finding the associated unsatisfied configuration of the smallest size. In the two- and three-qubit spaces these smallest-size unsatisfied configurations were found for all relevant sub-geometries. The first open case is – as already pointed out in Section 5.1 – the four-qubit one, in particular its elliptic quadrics. Here, the smallest-size unsatisfied configuration of a  $Q^-(7,2)$ should share with each of its 136 quadratic  $\mathcal{W}(5,2)$ 's a copy of the split Cayley hexagon of order two (which is the smallest-size unsatisfied configuration of the whole  $\mathcal{W}(5,2)$ , see [30,42]); this is, however, not the case for the configuration we found. Similarly, the 1575-line unsatisfied configuration found for the whole space does not meet the requirement that it shares a copy of  $\mathcal{DW}(5,2)$  with each of its 136  $\mathcal{Q}^+(7,2)$ 's (see the end of Section 5.1). Moreover, the sub-geometries we have so far dealt with are rather simple in the sense that their degree of contextuality is the same irrespectively of the rank of multi-qubit W(2N-1,2) they are located in; therefore, in this case it is sufficient to analyse just their smallest rank representatives. However, there exists a large class of configurations that do not behave this way. In the three-qubit space, an example of such a geometry is the two-spread – a point-line incidence structure we get from the doily after removing one of its spreads of lines [35]; here, there exist copies that are contextual [30], but also others that are not [26]! A prominent representative in the four-qubit space is the dual of the split Cayley hexagon of order two; here, we found several contextual copies differing in both the size and structure of the corresponding unsatisfied configurations. Obviously, geometries of this class, which are basically not defined by algebraic equations, will be more difficult to handle as per their contextuality properties and we will have to employ some new guiding principles to facilitate our computer-aided search and make it also more effective. For example, we can take a quantum contextual configuration whose degree of contextuality is known, remove from it certain sets of observables and associated contexts and check contextual properties of this reduced configuration. Similarly, we can add to a given configuration some new observables and contexts and compare contextuality properties of this extended configuration with those of the parent one. Another task worth a closer look would be to take several contextual configurations in the same polar space, remove their common part and check the resulting configuration; if the latter is contextual, compare its unsatisfied part with each of the original configurations.

<sup>&</sup>lt;sup>5</sup>For the sake of completeness, it is worth mentioning that in PG(3, q), q > 2, there also exists a hyperbolic congruence, i. e., the congruence consisting of  $(q+1)^2$  lines incident to two skew lines, which is shared by q-1 different polarities.

## 7 Conclusion

To conclude this work, it is also desirable to say a few words about the significance of studying general N-qubit proofs of quantum contextuality. Apart from its key role in the foundational issues of quantum mechanics, contextuality has also been recognized as a necessary resource for quantum computing, as in models based on magic state distillation, measurement-based quantum computation or in computational models of qubits [1]. Recently [11], it was further shown that for any quantum state and observables of sufficiently small dimensions producing contextuality, there exists a communication task with quantum advantage and that given any set of observables allowing for quantum state-independent contextuality, there exists a class of communication tasks wherein the difference between classical and quantum communication complexities increases as the number of inputs grows. As our approach quantifies observable-based proofs of contextuality, an interesting task would be to ascertain the perspective if this difference could eventually be expressed in terms of (or at least loosely linked to the notion of) the degree of contextuality. That this may be a viable task seems to be backed by [2], where contextuality of magic states was established as a necessary resource for a large class of quantum computation schemes based on qubits. Moreover, being already able to handle contextuality in symplectic spaces of several different ranks (and so the corresponding Hilbert spaces of different dimensions), we can also spot some dimension-sensitive features of contextual behavior – this also being in line with some seemingly unrelated recent research, like [52].

Beyond the application to quantum contextuality presented in this paper, our heuristic could also be competitive against other methods in other applications formalizable with XOR clauses, such as algebraic cryptanalysis [46] or discrete integration, which is a fundamental problem in numerous areas of artificial intelligence, including probabilistic reasoning, machine learning and planning [45]. This requires a deeper study of its own beyond the scope of this paper, being thus left as an interesting perspective.

## Acknowledgments

This work was supported in part by the Slovak VEGA grant agency, project number 2/0043/24, by the PEPR integrated project EPiQ ANR-22-PETQ-0007 part of Plan France 2030, by the EIPHI Graduate School (contract "ANR-17-EURE-0002") through the project TACTICQ. We would also like to cordially thank Dr. Violeta Felea (Université Marie et Louis Pasteur, Besançon, France), for her careful reading of the manuscript, Dr. Petr Pracna (Technology Centre, Prague) for the help with Figures 7, 9, 10, 11 and 12, Mr. Zsolt Szabó (Robert Bosch Kft, Budapest, Hungary) for the help with Figures 13 and 14, Dr. Henri de Boutray (ColibriTD, Paris) for creating for us the drawing of the Haar graph H(1103671145) as depicted in Figure 15 and, especially, Dr. Péter Vrana (Budapest University of Technology and Economics, Budapest, Hungary) for providing us with a particular labeling of the vertices of this graph in terms of five-qubit observables. Last but not least, we are also grateful to anonymous reviewers for their useful comments and suggestions towards improving the readability of our paper.

## Data Availability Statement

The data that support the findings of this study are openly available at the following URL/DOI: https://github.com/quantcert/quantcert.github.io/.

## A A particular bijection between three-qubit Fano planes and four-qubit observables

An explicit form of the bijection between 135 planes (each listed as a set of points/observables) of the three-qubit W(5,2) and 135 points/observables of the four-qubit hyperbolic quadric  $\mathcal{Q}^+_{IIII}(7,2)$  furnished by the LGr(3,6), which was employed in Section 5 to figure out basic properties of unsatisfied configurations of both a hyperbolic quadric and the whole four-qubit symplectic polar space W(7,2). For the reader's convenience, planes 1 to 105 are consecutively arranged into seven sets of 15 elements each, the planes in each such set passing through the same point/observable (listed first and separated by a semicolon from the rest); the corresponding seven 'first' observables pairwise anticommute and represent a particular Conwell heptad of  $\mathcal{Q}^+_{III}(5,2)$  (for the definition of a Conwell heptad in the three-qubit setting, see, e. g., [41]).

No.	Fano plane in $W(5,2)$	Point on $Q^+(7,2)$
1	$\{IIY; XYI, ZXY, XYY, ZXI, YZY, YZI\}$	YZXY
2	$\{IIY; XYI, YXI, XYY, YXY, ZZI, ZZY\}$	ZYYX
3	$\{IIY; XYI, IYI, XYY, IYY, XII, XIY\}$	XXZZ
4	$\{IIY; XXY, ZYI, XXI, ZYY, YZY, YZI\}$	XYYZ
5	$\{IIY; XXY, YYY, XXI, YYI, ZZI, ZZY\}$	IYYI
6	$\{IIY; XXY, IXY, XXI, IXI, XII, XIY\}$	XIIZ
7	$\{IIY; YII, IZY, YIY, IZI, YZY, YZI\}$	ZXZX
8	$\{IIY; YII, YYY, YIY, YYI, IYY, IYI\}$	YYYY
9	$\{IIY; YII, IXY, YIY, IXI, YXY, YXI\}$	XZXZ
10	$\{IIY; ZIY, IZY, ZII, IZI, ZZI, ZZY\}$	ZIIX
11	$\{IIY; ZIY, ZYI, ZII, ZYY, IYY, IYI\}$	ZZXX
12	$\{IIY; ZIY, IXY, ZII, IXI, ZXI, ZXY\}$	IZXI
13	$\{IIY; XZY, IZY, XZI, IZI, XII, XIY\}$	IXZI
14	$\{IIY; XZY, ZYI, XZI, ZYY, YXY, YXI\}$	YXZY
15	$\{IIY; XZY, YYY, XZI, YYI, ZXI, ZXY\}$	YIIY
16	$\{ZYX; YIZ, ZXY, XYY, IZZ, XXX, YZI\}$	IXYY
17	$\{ZYX; YIZ, YXI, XYY, XZX, IXZ, ZZY\}$	YYIZ
18	$\{ZYX; YIZ, IYI, XYY, ZIX, YYZ, XIY\}$	YZYX
19	$\{ZYX; YZX, ZYI, XXI, IIX, XXX, YZI\}$	XZZI
20	$\{ZYX; YZX, YYY, XXI, XIZ, IXZ, ZZY\}$	XXXZ
21	$\{ZYX; YZX, IXY, XXI, ZZZ, YYZ, XIY\}$	IYYZ
22	$\{ZYX; XYZ, IZY, YIY, ZXZ, XXX, YZI\}$	XYXY
23	$\{ZYX; XYZ, YYY, YIY, XIZ, ZIX, IYI\}$	YIYI
24	$\{ZYX; XYZ, IXY, YIY, ZZZ, XZX, YXI\}$	ZYZY
25	$\{ZYX;IYX,IZY,ZII,ZXZ,IXZ,ZZY\}$	ZZXI
26	$\{ZYX;IYX,ZYI,ZII,IIX,ZIX,IYI\}$	IZIX
27	$\{ZYX;IYX,IXY,ZII,ZZZ,IZZ,ZXY\}$	ZIXX
28	$\{ZYX; YXX, IZY, XZI, ZXZ, YYZ, XIY\}$	YXIY
29	$\{ZYX; YXX, ZYI, XZI, IIX, XZX, YXI\}$	XIZX
30	$\{ZYX; YXX, YYY, XZI, XIZ, IZZ, ZXY\}$	ZXZZ

No.	Fano plane in $W(5,2)$	Point on $Q^+(7,2)$
31	$\{YIX; ZYZ, ZXY, XYY, XXZ, IZX, YZI\}$	YYZI
32	$\{YIX; ZYZ, YXI, XYY, IXX, XZZ, ZZY\}$	XIYY
33	$\{YIX; ZYZ, IYI, XYY, YYX, ZIZ, XIY\}$	ZYXY
34	$\{YIX; YZX, YII, IZI, IIX, IZX, YZI\}$	IIZX
35	$\{YIX; YZX, ZIY, IZI, XIZ, XZZ, ZZY\}$	ZXZI
36	$\{YIX; YZX, XZY, IZI, ZZZ, ZIZ, XIY\}$	ZXIX
37	$\{YIX; XYZ, XXY, ZYY, ZXZ, IZX, YZI\}$	YYIX
38	$\{YIX; XYZ, ZIY, ZYY, XIZ, YYX, IYI\}$	YXYZ
39	$\{YIX; XYZ, XZY, ZYY, ZZZ, IXX, YXI\}$	IZYY
40	$\{YIX; IYX, XXY, YYI, ZXZ, XZZ, ZZY\}$	YXXY
41	$\{YIX;IYX,YII,YYI,IIX,YYX,IYI\}$	XZZX
42	$\{YIX; IYX, XZY, YYI, ZZZ, XXZ, ZXY\}$	ZYYZ
43	$\{YIX; YXX, XXY, IXI, ZXZ, ZIZ, XIY\}$	IZXZ
44	$\{YIX; YXX, YII, IXI, IIX, IXX, YXI\}$	XZII
45	$\{YIX; YXX, ZIY, IXI, XIZ, XXZ, ZXY\}$	XIXZ
46	$\{YZZ; ZYZ, ZYI, XXI, XXZ, IIZ, YZI\}$	IXXZ
47	$\{YZZ; ZYZ, YYY, XXI, IXX, XIX, ZZY\}$	XZZZ
48	$\{YZZ; ZYZ, IXY, XXI, YYX, ZZX, XIY\}$	XYYI
49	$\{YZZ; YIZ, YII, IZI, IZZ, IIZ, YZI\}$	ZXII
50	$\{YZZ; YIZ, ZIY, IZI, XZX, XIX, ZZY\}$	IXZX
51	$\{YZZ; YIZ, XZY, IZI, ZIX, ZZX, XIY\}$	ZIZX
52	$\{YZZ; XYZ, XYI, ZXI, ZXZ, IIZ, YZI\}$	ZIXZ
53	$\{YZZ; XYZ, ZIY, ZXI, XZX, YYX, IXY\}$	YZIY
54	$\{YZZ; XYZ, XZY, ZXI, ZIX, IXX, YYY\}$	XZXX
55	$\{YZZ; IYX, XYI, YXY, ZXZ, XIX, ZZY\}$	XYIY
56	$\{YZZ; IYX, YII, YXY, IZZ, YYX, IXY\}$	ZXYY
57	$\{YZZ; IYX, XZY, YXY, ZIX, XXZ, ZYI\}$	$YZYI \ YYXX$
58 59	$\{YZZ; YXX, XYI, IYY, ZXZ, ZZX, XIY\}$	IIYY
60	$\{YZZ; YXX, YII, IYY, IZZ, IXX, YYY\}$ $\{YZZ; YXX, ZIY, IYY, XZX, XXZ, ZYI\}$	YYZZ
61		$\frac{1}{YZYZ}$
62	$\{XYX; ZYZ, YYY, YIY, ZIZ, XIX, IYI\}$	IYIY
63	$\{XYX;ZYZ,IXY,YIY,XZZ,ZZX,YXI\}$	YXYX
64	$\{XYX;YIZ,XXY,ZYY,IZZ,ZXX,YZI\}$	ZIYY
65	$\{XYX;YIZ,ZIY,ZYY,YYZ,XIX,IYI\}$	XYZY
66	$\{XYX;YIZ,XZY,ZYY,IXZ,ZZX,YXI\}$	YYXI
67	$\{XYX;YZX,XYI,ZXI,IIX,ZXX,YZI\}$	XZIX
68	$\{XYX;YZX,ZIY,ZXI,YYZ,XZZ,IXY\}$	YIXY
69	$\{XYX;YZX,XZY,ZXI,IXZ,ZIZ,YYY\}$	ZZXZ
70	$\{XYX; IYX, XYI, XII, IIX, XIX, IYI\}$	XIZI
71	$\{XYX; IYX, XXY, XII, IZZ, XZZ, IXY\}$	IXZZ
72	$\{XYX; IYX, XZY, XII, IXZ, XXZ, IZY\}$	XXIZ
73	$\{XYX;YXX,XYI,ZZI,IIX,ZZX,YXI\}$	IZZX
74	$\{XYX; YXX, XXY, ZZI, IZZ, ZIZ, YYY\}$	ZXXX
75	$\{XYX; YXX, ZIY, ZZI, YYZ, XXZ, IZY\}$	ZYYI
75	$\{A Y A; Y A A, Z IY, Z Z I, Y Y Z, X X Z, I Z Y\}$	ZYYI

No.	Fano plane in $W(5,2)$	Point on $Q^+(7,2)$
76	$\{IYZ; ZYZ, IZY, ZII, IXX, ZXX, ZZY\}$	IZXX
77	$\{IYZ;ZYZ,ZYI,ZII,ZIZ,IIZ,IYI\}$	ZIXI
78	$\{IYZ;ZYZ,IXY,ZII,IZX,ZZX,ZXY\}$	ZZIX
79	$\{IYZ; YIZ, XXY, YYI, XZX, ZXX, ZZY\}$	YZZY
80	$\{IYZ;YIZ,YII,YYI,YYZ,IIZ,IYI\}$	ZXXZ
81	$\{IYZ; YIZ, XZY, YYI, XXX, ZZX, ZXY\}$	XYYX
82	$\{IYZ; YZX, XYI, YXY, XIZ, ZXX, ZZY\}$	YIYZ
83	$\{IYZ;YZX,YII,YXY,YYZ,IZX,IXY\}$	YYZX
84 85	$\{IYZ;YZX,XZY,YXY,XXX,ZIZ,ZYI\}$	$IYXY \ IXIZ$
86	$\{IYZ; XYZ, XYI, XII, XIZ, IIZ, IYI\}$ $\{IYZ; XYZ, XXY, XII, XZX, IZX, IXY\}$	XXZI
87	$\{IYZ; XYZ, XZY, XII, XZX, IZX, IXY\}$	XIZZ
88	$\{IYZ; YXX, XYI, YZY, XIZ, ZZX, ZXY\}$	XIZZ $YXYI$
89	$\{IYZ; YXX, XXY, YZY, XZX, ZIZ, ZYI\}$	ZYIY
90	$\{IYZ; YXX, YII, YZY, YYZ, IXX, IZY\}$	XZYY
91	$\{YXZ; ZYZ, IZY, XZI, YYX, ZXX, XIY\}$	YIZY
92	$\{YXZ; ZYZ, ZYI, XZI, XZZ, IIZ, YXI\}$	ZXIZ
93	$\{YXZ; ZYZ, YYY, XZI, IZX, XIX, ZXY\}$	XXZX
94	$\{YXZ;YIZ,XXY,IXI,ZIX,ZXX,XIY\}$	XZXI
95	$\{YXZ;YIZ,YII,IXI,IXZ,IIZ,YXI\}$	IIXZ
96	$\{YXZ;YIZ,ZIY,IXI,XXX,XIX,ZXY\}$	XZIZ
97	$\{YXZ; YZX, XYI, IYY, ZZZ, ZXX, XIY\}$	ZZYY
98	$\{YXZ; YZX, YII, IYY, IXZ, IZX, YYY\}$	YYII
99	$\{YXZ;YZX,ZIY,IYY,XXX,XZZ,ZYI\}$	XXYY
100 101	$\{YXZ; XYZ, XYI, ZZI, ZZZ, IIZ, YXI\}$	$ZXXI \ ZZZX$
101	$\{YXZ; XYZ, XXY, ZZI, ZIX, IZX, YYY\} $ $\{YXZ; XYZ, ZIY, ZZI, XXX, YYX, IZY\}$	IYYX
102	$\{YXZ; IYX, XYI, YZY, ZZZ, XIX, ZXY\}$	IYZY
103	$\{YXZ; IYX, XXY, YZY, ZIX, XZZ, ZYI\}$	YIYX
105	$\{YXZ; IYX, YII, YZY, IXZ, YYX, IZY\}$	YYXZ
106	$\{XXI,IIX,IXX,XXX,XIX,IXI,XII\}$	XIII
107	$\{ZII, ZZZ, IZI, IZZ, ZZI, ZIZ, IIZ\}$	ZIII
108	$\{ZXZ,YIY,XZZ,XXX,YYI,ZZX,IYY\}$	XXXX
109	$\{XXZ, XIZ, YXY, IXI, ZIX, ZXX, YIY\}$	XIXI
110	$\{ZZX, YYX, IXZ, XXI, ZYY, YZY, XIZ\}$	XXXI
111	$\{ZXX,ZXI,YYI,IIX,XZX,XZI,YYX\}$	XIIX
112	$\{YZY, YYZ, ZIX, IXX, XZZ, XYY, ZXI\}$	XIXX
113	$\{XZI, IZX, ZYY, XIX, YXY, ZXZ, YYZ\}$	XXIX
114	$\{XYY, XZX, YYX, IXZ, ZIZ, ZXI, YZY\}$	ZZIZ
115	$\{ZXZ, XZZ, ZXI, YYI, IIZ, YYZ, XZI\}$	ZIIZ
116	$\{XXZ,YXY,YYZ,ZIX,ZZI,IZX,XYY\}$	$ZZZI \ ZZII$
117 118	$\{ZZX, IXZ, IZX, ZYY, ZII, IYY, ZXZ\} \ \{ZXX, YYI, IYY, XZX, ZZZ, YIY, XXZ\}$	ZZZZ
119	$\{YZY, ZIX, YIY, XZZ, IZI, XIZ, ZZX\}$	ZIZI
120	$\{ZZZ, IZZ, IXX, ZII, ZYY, IYY, ZXX\}$	IIXX
121	$\{IZI, ZIZ, XIX, ZZZ, XZX, YIY, YZY\}$	IXIX

No.	Fano plane in $\mathcal{W}(5,2)$	Point on $Q^+(7,2)$
122	$\{IZZ, IIZ, XII, IZI, XZZ, XIZ, XZI\}$	IXII
123	$\{ZIZ, ZZI, XXX, IZZ, YXY, YYX, XYY\}$	IXXX
124	$\{IIZ,ZII,IXI,ZIZ,IXZ,ZXI,ZXZ\}$	IIXI
125	$\{ZZI, ZZZ, XXI, IIZ, YYI, YYZ, XXZ\}$	IXXI
126	$\{IIX, XXI, YYX, XXX, YYI, ZZX, ZZI\}$	IZZI
127	$\{IXX,IIX,ZXI,IXI,ZIX,ZXX,ZII\}$	IZII
128	$\{XIX, IXX, YYZ, XXI, ZYY, YZY, ZZZ\}$	IZZZ
129	$\{XII,XIX,IZX,IIX,XZX,XZI,IZI\}$	IIZI
130	$\{XXX,XII,IYY,IXX,XZZ,XYY,IZZ\}$	IIZZ
131	$\{IXI, XXX, YIY, XIX, YXY, ZXZ, ZIZ\}$	IZIZ
132	$\{XYY,IYY,XZX,XII,IXZ,XXZ,IZX\}$	XXII
133	$\{XZI, ZYY, XIZ, YXY, IZZ, YYX, ZXX\}$	ZIZZ
134	$\{ZII,IZI,IIX,ZZI,ZIX,IZX,ZZX\}$	IIIX
135	$\{XXI,IXI,XIZ,XII,IXZ,XXZ,IIZ\}$	IIIZ

## B Experiments for parameter optimization

Figures 17, 18 and 19 display, in a form of heatmaps, the best Hamming distances computed by runs of Algorithm 1 with 100 iterations, for various specific values of the flip probability,  $\gamma$ , and the threshold,  $\theta$ , and a variety of different input configurations. The warm-to-cool color scheme (and the associated numbers) of cells shows the variation of the corresponding Hamming distance, with dark blue indicating its lowest values and dark red its highest ones. In Figure 17a (respectively 17b and 18), the input configuration is the whole set of lines in the three- (respectively four- and five-)qubit symplectic polar space. For Figures 19a, 19b and 19c, the input configurations are, respectively, the subsets of the three-qubit space composed of its 80, 180 and 280 lexicographically smallest lines, when these lines are totally ordered by the lexicographic order defined in the subsequent paragraph.

We briefly recall here the definition of the lexicographic order introduced in a former work [28] to break symmetry in quantum configurations. Let < denote the total order on the alphabet  $\{I, X, Y, Z\}$  defined by I < X < Z < Y. Let us also denote by < its lexicographic extension to Pauli observables, considered as words on this alphabet. With the same notation <, this order can be further extended to all tuples  $(a_1, a_2, \ldots, a_n)$  of Pauli observables, by ordering them with < applied to the Pauli observable  $a_1 a_2 \ldots a_n$ . This order can also be defined over finite sets  $\{a_1, a_2, \ldots, a_n\}$  of Pauli observables, by canonically associating to each set the tuple  $(a_1, a_2, \ldots, a_n)$  of its elements written in increasing order  $(a_i < a_j \text{ when } i < j)$ , and so on, at any level of the hierarchy of objects of the same nature, such as configurations that are sets of lines and that are themselves sets of Pauli observables.

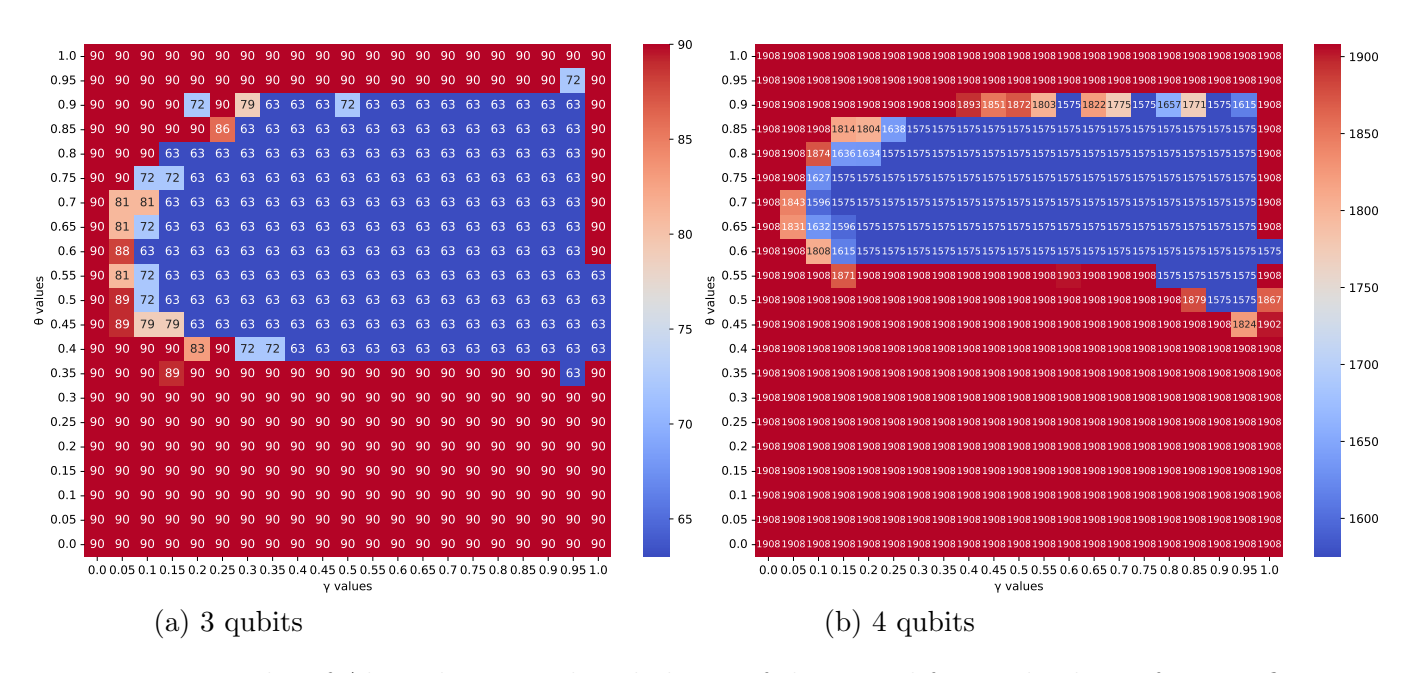


Figure 17: Results of Algorithm 1 on the whole set of three- and four-qubit lines, for specific values of  $\theta$  and  $\gamma$ .

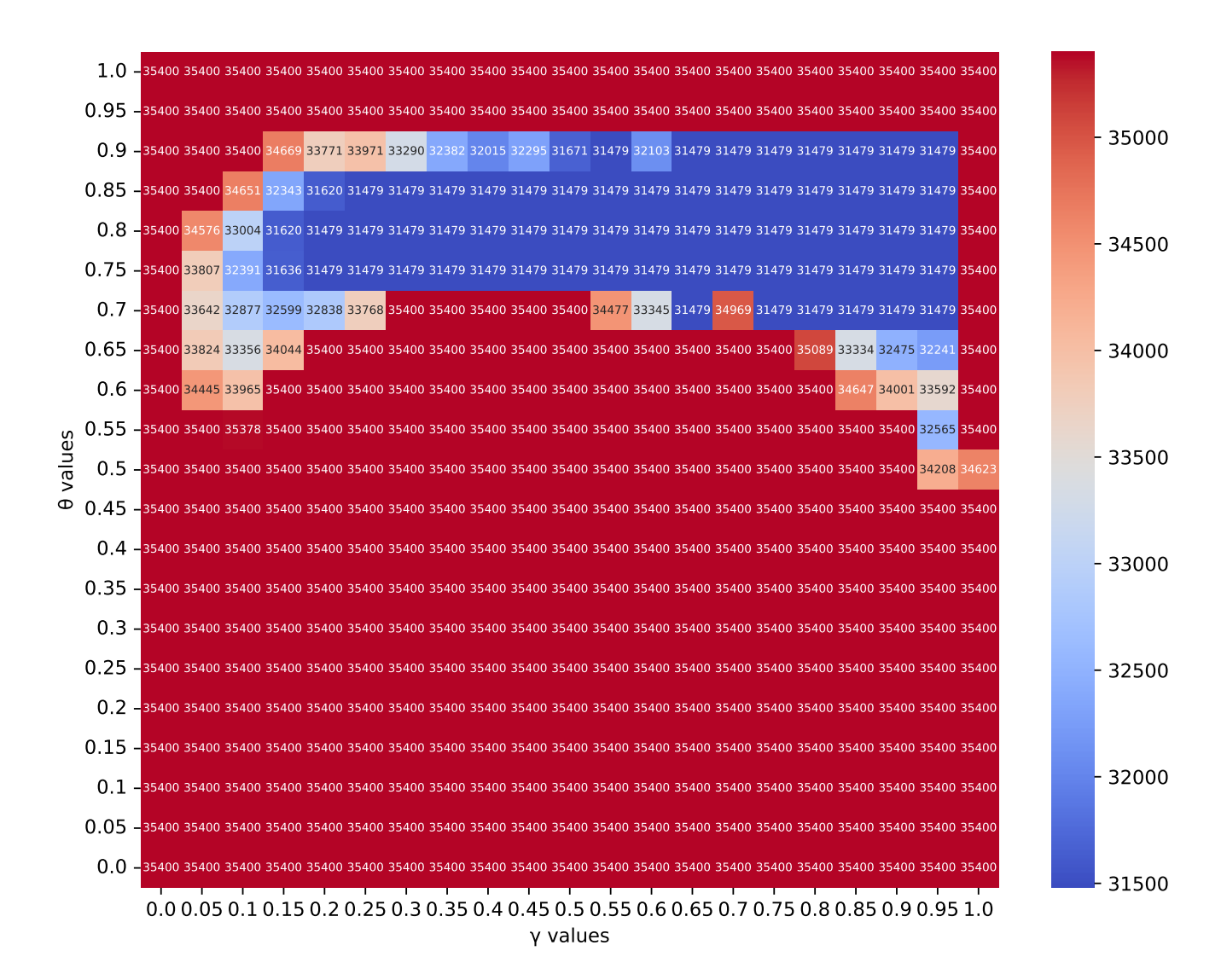
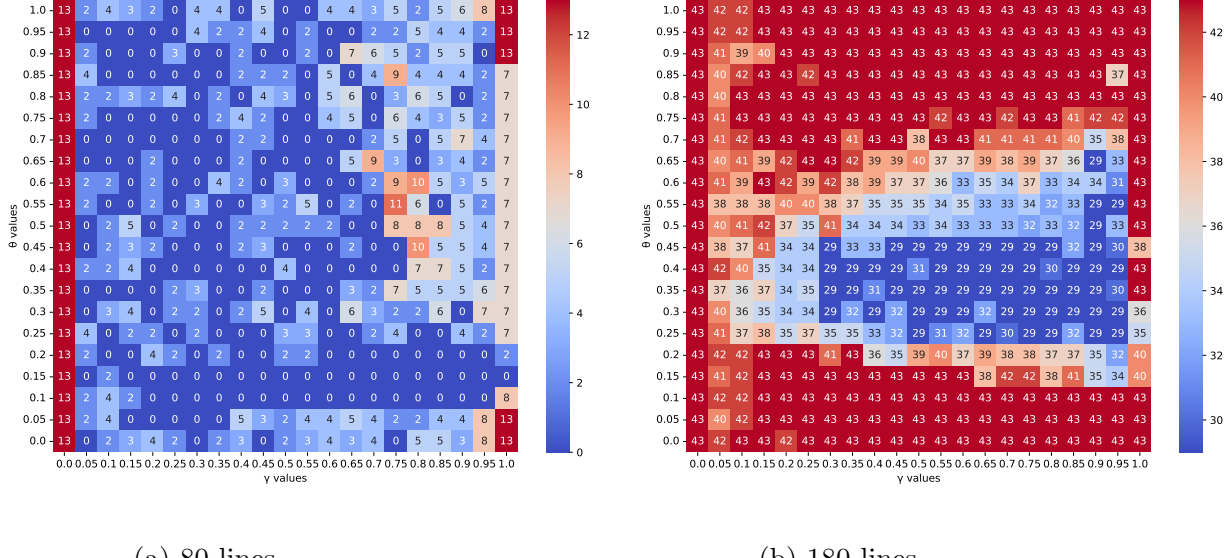


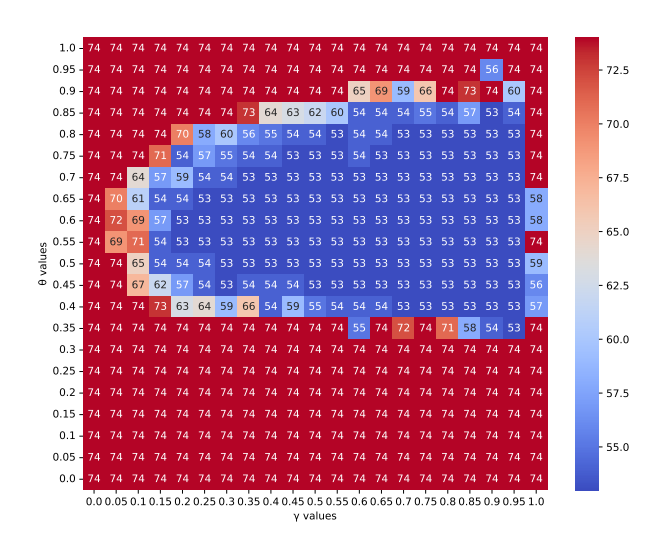
Figure 18: Results of Algorithm 1 on the whole set of five-qubit lines, for specific values of  $\theta$  and  $\gamma$ .

If  $\gamma=0$ , the algorithm never flips any value, and the initial assignment is kept. If  $\gamma=1$ , the algorithm always flips the value if it is above the threshold  $\theta$ , making it deterministic and increasing the probability of cycling through of a (possibly substantially small) subset of states. The shape of the blue areas in the heatmaps of the experimental results suggests that any sufficiently high value of  $\gamma$  lets the algorithm reach small Hamming distances for approximately the same range of heights of values of  $\theta$ . Therefore, the algorithm works with a fixed value of  $\gamma$ .

Since the presented experimental results show that the optimal values of  $\theta$  can vary significantly depending on the input (see Figure 19), we decided to dynamically adjust the value of  $\theta$  during the computational process of the algorithm. Moreover, when  $\gamma$  is high enough, most of the optimal values of  $\theta$  are in a single interval, whose bounds are the high and low horizontal limits of the blue areas in the heatmaps of the experimental results. This observation suggests that the algorithm should be capable of adjusting



(a) 80 lines (b) 180 lines



(c) 280 lines

Figure 19: Benchmark results for specific values of  $\theta$  and  $\gamma$  on certain subsets of the set of three-qubit lines.

these bounds during its execution.

## C Tool results and performances

This appendix collects the exact values or upper bounds of contextuality degrees computed by our algorithm as well as by the other approaches presented in Section 3.1, together with their computation time, for a variety of quantum configurations.

Table 4 summarizes all the experimental data. The input configurations are described in the first column and grouped by number of qubits. They include elliptic  $(\mathcal{Q}^-(\ldots,2))$  and hyperbolic  $(\mathcal{Q}^+(\ldots,2))$  quadrics, the full sets of lines of polar spaces of rank three to five  $(\mathcal{W}(\ldots,2))$  and the complement of a skew-embedded three-qubit split Cayley hexagon of order two,  $\overline{\mathcal{H}}_{\mathcal{S}}$ . The remaining configurations are subsets of lines of the three-qubit space  $\mathcal{W}(5,2)$ , composed of the l smallest lines according to the lexicographic order introduced in B. Thus, every subset is constructed as a subset of the next one in order to study the evolution of the computation time when the size of the input configuration grows. Moreover, these inclusions of subsets entail that the difficulty in computing the degree of contextuality or its upper bound increases with increasing numbers of lines – a fact well confirmed by the experimental results.

The next two columns of Table 4 present, respectively, the number of observables p and the number of contexts/lines l in a given configuration. The fourth column displays the contextuality degree d found, or its best-known upper bound when preceded by the symbol  $\leq$ . The fifth and sixth columns give, respectively, the dimension (dim) and codimension (codim) of the incidence matrix of the configuration, the two parameters that are essential for evaluating the performance of the Magma approach. The columns Magma, SAT(x) [30] and OR-Tools(x) display the time taken by the corresponding exact approaches to confirm that a given bound is the lowest (i. e., the contextuality degree), whereas the columns SAT(a), OR-Tools(a) and heuristic display the time taken to find the same number without checking its minimality. The times are given in seconds unless otherwise specified. A prolonged dash ('—') represents the time duration considered too long to be measured, typically more than 24 hours. The calculations were performed on an Intel(R) Core(TM) i7-12700H processor with 20 cores and 16 Gb of RAM.

In the first block (set of rows) of Table 4 the number of lines l of the subsets of the three-qubit space ranges from 70 to 87 in order to mainly demonstrate the performance limits of the Magma approach. Similarly, l varies from 100 to 190 in the third block of Table 4 in order to illustrate the performance limits for the SAT- and OR-Tools-based exact approaches SAT(x) and OR-Tools(x). We opted here for a larger gap of ten contexts between individual sets because here the complexity increases less rapidly when compared with that characterizing the Magma approach. The penultimate block of rows shows the limit of the approximate SAT-based approach SAT(a). The last block shows the limits of all the methods except the heuristic one.

Configuration	p	l	d	dim	codim	Magma	SAT(x)	OR-Tools(x)	SAT(a)	$OR ext{-}Tools(a)$	heuristic
3-qubit lines	63	70	0	44	26	0.07	0.1	< 0.01	0.03	< 0.01	< 0.01
3-qubit lines	63	71	0	44	27	0.14	0.1	< 0.01	0.02	< 0.01	< 0.01
3-qubit lines	63	72	0	45	27	0.14	0.1	0.01	0.06	0.01	< 0.01
3-qubit lines	63	73	0	45	28	0.26	0.1	0.01	0.09	0.01	< 0.01
3-qubit lines	63	74	0	46	28	0.28	0.1	0.01	0.04	0.01	< 0.01
3-qubit lines	63	75	0	46	29	0.52	0.1	0.02	0.08	0.02	< 0.01
3-qubit lines	63	76	0	46	30	1.04	0.1	0.02	0.10	0.02	< 0.01
3-qubit lines	63	77	0	46	31	2.05	0.1	0.02	0.08	0.02	< 0.01
3-qubit lines	63	78	0	46	32	4.32	0.1	0.02	0.03	0.02	< 0.01
3-qubit lines	63	79	0	46	33	8.55	0.1	0.02	0.02	0.02	< 0.01
3-qubit lines	63	80	0	46	34	16.5	0.1	0.02	0.07	0.02	< 0.01
3-qubit lines	63	81	0	46	35	32.4	0.1	0.02	0.12	0.02	< 0.01
3-qubit lines	63	82	0	46	36	1m6	0.1	0.02	0.10	0.02	< 0.01
3-qubit lines	63	83	0	46	37	1m22	0.1	0.03	0.14	0.03	< 0.01
3-qubit lines	63	84	0	46	38	4m22	0.1	0.03	0.17	0.03	< 0.01
3-qubit lines	63	85	0	46	39	9m01	0.1	0.04	0.12	0.04	< 0.01
3-qubit lines	63	86	0	46	40	17m56	0.1	0.04	0.01	0.04	< 0.01
3-qubit lines	63	87	0	46	41	34m23	0.1	0.04	0.12	0.04	< 0.01
$Q^{-}(5,2)$	27	45	9	21	24	0.02	0.3	0.7	0.07	0.5	0.01
$Q^{+}(5,2)$	35	105	21	29	76	9	13	11m31	0.5	0.01	0.01
compl. of $\mathcal{H}_{\mathcal{S}}$	63	252	24	56	196	_	50	1.5	9.7	0.01	0.01
3-qubit lines	63	100	0	51	49	_	0.1	0.1	0.1	0.01	0.01
3-qubit lines	63	110	3	54	56	_	0.1	0.15	0.1	0.01	0.7
3-qubit lines	63	120	8	55	65	_	0.5	0.02	0.3	0.02	0.02
3-qubit lines	63	130	12	55	75	_	4.4	0.16	2.8	0.07	0.01
3-qubit lines	63	140	15	55	85	_	42.0	0.2	24.6	0.06	0.01
3-qubit lines	63	150	20	55	95	_	5m44	3.2	3m10	0.24	0.04
3-qubit lines	63	160	24	55	105	_	7m49	6.1	1m18	0.16	0.07
3-qubit lines	63	170	27	55	115		21m48	53	13m55	0.22	0.01
3-qubit lines	63	180	29	55	125	_	1h20m	1m8	48m12	0.45	0.01
3-qubit lines	63	190	31	56	134	_	1h12m	1h18	13m07	0.51	0.03
$\mathcal{W}(5,2)$	63	315	63	56	259	_	19h	—(>30h)	13m55	0.7	0.01
$Q^{-}(7,2)$	119	1071	<315	111	960	_		_	_	8.3	0.01
$\mathcal{Q}^+(7,2)$	135	1575	 ≤315	127	1448		_	_	_	8.7	0.01
$\widetilde{\mathcal{W}}(7,2)$	255	5355	 ≤1575	246	5109	_	_	_	_	1m40	0.01
$Q^{-}(9,2)$	495	19635	≤7087	485	19150	_	_	_	_	_	0.1
$Q^{+}(9,2)$	527	23715	_ ≤6975	517	23198	_		_	_	_	0.1
$\mathcal{W}(9,2)$	1023	86955	$\leq 31479$	1012	85943	_				_	0.4

Table 4: A comparison of the performance of Magma-, SAT-, OR-Tools- and heuristic-based minimizers in computing the contextuality degree of distinguished configurations in symplectic polar spaces of rank three to five as well as of specific sets of lines in the three-qubit space.

## References

- [1] B. Amaral, Resource theory of contextuality, Philosophical Transactions of the Royal Society A 377 (2019), 20190010. https://doi.org/10.1098/rsta.2019.0010.
- [2] J. Bermejo-Vega, N. Delfosse, D. E. Browne, C. Okay, and R. Raussendorf, Contextuality as a resource for models of quantum computation with qubits, Physical Review Letters 119 (2017), 120505. https://doi.org/10.1103/PhysRevLett.119.120505.
- [3] K. Coolsaet, The smallest split Cayley hexagon has two symplectic embeddings, Finite Fields and Their Applications 16 (2010), 380–384. https://doi.org/10.1016/j.ffa. 2010.06.003.
- [4] H. S. M. Coxeter, My graph, Proceedings of the London Mathematical Society 46 (1983), 117–136. https://doi.org/10.1112/plms/s3-46.1.117.
- [5] H. de Boutray, F. Holweck, A. Giorgetti, P.-A. Masson, and M. Saniga, Contextuality degree of quadrics in multi-qubit symplectic polar spaces, Journal of Physics A: Mathematical and Theoretical 55 (2022), no. 47, 475301. https://doi.org/10.1088/1751-8121/aca36f.
- [6] B. de Bruyn, The hyperplanes of  $DW(5, 2^h)$  which arise from embedding, Discrete Mathematics 309 (2009), 304–321. https://doi.org/10.1016/j.disc.2007.12.011.
- [7] \_\_\_\_\_, An introduction to incidence geometry, Birkhäuser, 2016. https://link.springer.com/book/10.1007/978-3-319-43811-5.
- [8] P. Dembowski, Finite geometries, Springer-Verlag, 1968. https://link.springer.com/book/10.1007/978-3-642-62012-6.
- [9] W. L. Edge, The geometry of the linear fractional group LF(4,2), Proceedings of the London Mathematical Society **3-4** (1954), 317–342. https://doi.org/10.1112/plms/s3-4.1.317.
- [10] D. Frohardt and P. Johnson, Geometric hyperplanes in generalized hexagons of order (2, 2), Communications in Algebra 22 (1994), no. 3, 773–797. https://doi.org/10.1080/00927879408824875.
- [11] S. Gupta, D. Saha, Z.-P. Xu, A. Cabello, and A. S. Majumdar, *Quantum contextuality provides communication complexity advantage*, Physical Review Letters **130** (2023), 080802. https://doi.org/10.1103/PhysRevLett.130.080802.
- [12] H. Havlicek, B. Odehnal, and M. Saniga, Factor-group-generated polar spaces and (multi)-qudits, SIGMA (Symmetry, Integrability and Geometry: Methods and Applications) 5 (2009), 096. https://doi.org/10.3842/SIGMA.2009.096.
- [13] P. J. Heawood, Map-colour theorem, The Quarterly Journal of Pure and Applied Mathematics 24 (1890), 332–338. https://gdz.sub.uni-goettingen.de/id/PPN600494829\_0024.
- [14] J. W. P. Hirschfeld, Finite projective spaces of three dimensions, Oxford University Press, 1985. https://books.google.fr/books?id=EzLZy9\_N6jOC.
- [15] \_\_\_\_\_, Projective geometries over finite fields, Oxford University Press, 1998. https://doi.org/10.1093/oso/9780198502951.001.0001.
- [16] J. W. P. Hirschfeld and J. A. Thas, General Galois geometries, Springer, 2016. https://link.springer.com/book/10.1007/978-1-4471-6790-7.
- [17] F. Holweck, H. de Boutray, and M. Saniga, Three-qubit-embedded split Cayley hexagon is contextuality sensitive, Scientific Reports 12 (2022), no. 1, 8915. https://doi.org/10.1038/s41598-022-13079-3.
- [18] F. Holweck, M. Saniga, and P. Lévay, A notable relation between N-qubit and  $2^{N-1}$ -qubit Pauli groups via binary LGr(N, 2N), SIGMA (Symmetry, Integrability and Geometry: Methods and Applications) 10 (2014), 041. https://doi.org/10.3842/SIGMA.2014.041.

- [19] J. Håstad, Some optimal inapproximability results, Journal of the Association for Computing Machinery 48 (2001), no. 4, 798–859. https://doi.org/10.1145/502090.502098.
- [20] G. Kiss and T. Szönyi, *Finite geometries*, Taylor and Francis, 2020. https://www.routledge.com/Finite-Geometries/Kiss-Szonyi/p/book/9781032475387?srsltid=AfmBOootKiPtuwy8h5MpKATD8PYvDzi5xnWpJRsJgv04aL-ZkfNaqtAy.
- [21] P. Lévay, M. Planat, and M. Saniga, Grassmannian connection between three- and four-qubit observables, Mermin's contextuality and black holes, Journal of High Energy Physics 9 (2013), 037. https://doi.org/10.1007/JHEP09(2013)037.
- [22] P. Lévay, M. Saniga, and P. Vrana, Three-qubit operators, the split Cayley hexagon of order two and black holes, Physical Review D 78 (2008), no. 12, 124022. https://doi.org/10. 1103/PhysRevD.78.124022.
- [23] P. Lévay and Z. Szabó, Mermin pentagrams arising from Veldkamp lines for three qubits, Journal of Physics A: Mathematical and Theoretical **50** (2017), no. 9, 095201. https://doi.org/10.1088/1751-8121/aa56aa.
- [24] N. D. Mermin, *Hidden variables and the two theorems of John Bell*, Reviews of Modern Physics **65** (1993), 803–815. https://doi.org/10.1103/RevModPhys.65.803.
- [25] M. Minichiello, Solving MAX-XOR-SAT problems with stochastic local search, Master's Thesis, 2002. Masters in Mathematics 3rd Year Project Report, University of York. https://citeseerx.ist.psu.edu/document?doi=9225c5c1e3801c94347a696b61345aa39fac546e.
- [26] A. Muller and A. Giorgetti, An abstract structure determines the contextuality degree of observable-based Kochen-Specker proofs, Journal of Mathematical Physics 66 (2025), no. 8, 082203. https://doi.org/10.1063/5.0245341.
- [27] \_\_\_\_\_\_, Qontextium, public GitHub repository, last accessed on May 5, 2025. Available online in the contextualityDegree folder at https://github.com/quantcert/quantcert.github.io/.
- [28] A. Muller, M. Saniga, A. Giorgetti, H. de Boutray, and F. Holweck, Multi-qubit doilies: Enumeration for all ranks and classification for ranks four and five, Journal of Computational Science 64 (October 2022), 101853. https://doi.org/10.1016/j.jocs.2022. 101853.
- [29] A. Muller, M. Saniga, A. Giorgetti, F. Holweck, and C. Kelleher, A new heuristic approach for contextuality degree estimates and its four- to six-qubit portrayals, Journal of Physics A: Mathematical and Theoretical 58 (2025), no. 21, 215302. https://doi.org/10.1088/ 1751-8121/add22b.
- [30] A. Muller, M. Saniga, A. Giorgetti, H. de Boutray, and F. Holweck, New and improved bounds on the contextuality degree of multi-qubit configurations, Mathematical Structures in Computer Science 34 (2024), no. 4, 322–343. https://doi.org/10.1017/S0960129524000057.
- [31] S. E. Payne and J. A. Thas, *Finite generalized quadrangles*, European Mathematical Society, 2009. https://doi.org/https://doi.org/10.4171/066.
- [32] L. Perron and V. Furnon, *OR-Tools*, Google, last accessed on July 5, 2024. Available online at https://developers.google.com/optimization.
- [33] M. Planat, M. Saniga, and F. Holweck, Distinguished three-qubit 'magicity' via automorphisms of the split Cayley hexagon, Quantum Information Processing 12 (2013), no. 7, 2535–2549. https://doi.org/10.1007/s11128-013-0547-3.
- [34] B. Polster and H. Van Maldeghem, Some constructions of small generalized polygons, Journal of Combinatorial Theory, Series A **96** (2001), 162–179. https://doi.org/10.1006/jcta.2001.3174.

- [35] B. Polster, *Pretty pictures of geometries*, Bulletin of the Belgian Mathematical Society Simon Stevin 5 (1998), no. 2/3, 417–425. https://doi.org/10.36045/bbms/1103409021.
- [36] B. Polster, A. E. Schroth, and H. Van Maldeghem, *Generalized flatland*, The Mathematical Intelligencer **23** (2001), 33–47. https://doi.org/10.1007/BF03024601.
- [37] H. Pralle, The hyperplanes of DW(5,2), Experimental Mathematics 14 (2005), 373–384. https://doi.org/10.1080/10586458.2005.10128922.
- [38] H. W. Richmond, The figure formed from six points in space of four dimensions, Mathematische Annalen 53 (1900), 161–176. https://doi.org/10.1007/BF01456032.
- [39] M. A. Ronan, Embeddings and hyperplanes of discrete geometries, European Journal of Combinatorics 8 (1987), 179–185. https://doi.org/10.1016/S0195-6698(87)80009-4.
- [40] M. Saniga, F. Holweck, and H. Jaffali, Taxonomy of three-qubit Mermin pentagrams, Symmetry 12 (2020), 534. https://doi.org/10.3390/sym12040534.
- [41] M. Saniga, H. de Boutray, F. Holweck, and A. Giorgetti, *Taxonomy of polar subspaces of multi-qubit symplectic polar spaces of small rank*, Mathematics **9** (2021), no. 18, 2272. https://doi.org/10.3390/math9182272.
- [42] M. Saniga, F. Holweck, C. Kelleher, A. Muller, A. Giorgetti, and H. de Boutray, *Hexagons govern three-qubit contextuality*, Quantum 9 (2025), 1601. https://doi.org/10.22331/q-2025-01-20-1601.
- [43] M. Saniga and M. Planat, Multiple qubits as symplectic polar spaces of order two, Advanced Studies in Theoretical Physics 1 (2007), 1–4. https://www.m-hikari.com/astp/astp2007/astp1-4-2007/sanigaASTP1-4-2007.pdf.
- [44] A. E. Schroth, *How to draw a hexagon*, Discrete Mathematics **199** (1999), no. 1–3, 161–171. https://doi.org/10.1016/S0012-365X(98)00294-5.
- [45] M. Soos and K. S. Meel, Gaussian elimination meets maximum satisfiability, Proceedings of the 18th International Conference on Principles of Knowledge Representation and Reasoning, 2021, pp. 581–587. https://doi.org/10.24963/kr.2021/55.
- [46] M. Soos, K. Nohl, and C. Castelluccia, Extending SAT solvers to cryptographic problems, Proceedings of the 12th International Conference on Theory and Applications of Satisfiability Testing, 2009, pp. 244–257. https://doi.org/10.1007/978-3-642-02777-2\_24.
- [47] K. Thas, The geometry of generalized Pauli operators of N-qudit Hilbert space, and an application to MUBs, EPL Europhysics Letters 86 (2009), 60005. https://doi.org/10.1209/0295-5075/86/60005.
- [48] S. Trandafir, P. Lisoněk, and A. Cabello, *Irreducible magic sets for n-qubit systems*, Phys. Rev. Lett. **129** (2022), 200401. https://doi.org/10.1103/PhysRevLett.129.200401.
- [49] \_\_\_\_\_, Irreducible magic sets for n-qubit systems, 2022. arXiv preprint https://arxiv.org/abs/2202.13141v2.
- [50] P. Vrana and P. Lévay, The Veldkamp space of multiple qubits, Journal of Physics A: Mathematical and Theoretical 43 (2010), no. 12, 125303. https://doi.org/10.1088/ 1751-8113/43/12/125303.
- [51] E. W. Weisstein, *Haar graph*, MathWorld A Wolfram Web Resource, last accessed on June 17, 2024. Available online at https://mathworld.wolfram.com/HaarGraph.html.
- [52] X.-D. Yu, I. Veeren, and O. Gühne, Characterizing high-dimensional quantum contextuality, Physical Review A 109 (2024), L030201. https://doi.org/10.1103/PhysRevA.109. L030201.